



Vibration and nonlinear dynamic analysis of sandwich FG-CNTRC plate with porous core layer

Ngo Dinh Dat , Nguyen Van Thanh , Vu MinhAnh & Nguyen Dinh Duc

To cite this article: Ngo Dinh Dat , Nguyen Van Thanh , Vu MinhAnh & Nguyen Dinh Duc (2020): Vibration and nonlinear dynamic analysis of sandwich FG-CNTRC plate with porous core layer, Mechanics of Advanced Materials and Structures, DOI: [10.1080/15376494.2020.1822476](https://doi.org/10.1080/15376494.2020.1822476)

To link to this article: <https://doi.org/10.1080/15376494.2020.1822476>



Published online: 29 Sep 2020.



Submit your article to this journal [↗](#)



View related articles [↗](#)



View Crossmark data [↗](#)

Vibration and nonlinear dynamic analysis of sandwich FG-CNTRC plate with porous core layer

Ngo Dinh Dat^a, Nguyen Van Thanh^{b,c}, Vu MinhAnh^c, and Nguyen Dinh Duc^{d,e}

^aFaculty of Automotive Mechanical and Electrical & Electronics Engineering (FAME), Nguyen Tat Thanh University, Ho Chi Minh City, Vietnam; ^bFaculty of Fundamental Sciences, Military Academy of Logistics, Ngoc Thuy, Long Bien, Hanoi, Vietnam; ^cDepartment of Technology and Engineering of Constructions and Transportation, VNU Hanoi – University of Engineering and Technology (UET), Hanoi, Vietnam; ^dInternational School of Vietnam, National University, Cau Giay, Ha Noi, Vietnam; ^eNational Research Laboratory, Department of Civil and Environmental Engineering, Sejong University, Gwangjin-gu, Seoul, South Korea

ABSTRACT

This paper focuses on the influence of CNTs, porosity, mechanical and thermal loading on the vibration and dynamic response of the sandwich functionally graded carbon nanotube-reinforced composite (FG-CNTRC) composite plate. The plate is made by three layers in which the core layer is porous FGM materials, bottom and top surfaces are FG-CNTRC. The motion equations are given based on Hamilton's principle, TSDT, Galerkin method and the fourth-order Runge–Kutta method. The numerical illustration is shown to examine the influence of various parameters such as porosity distribution, CNTs volume fraction, geometrical parameters, elastic foundations, temperature, mechanical loads on the dynamic behaviors of the plate.

HIGHLIGHTS

- The FG-CNTRC plates with porous core layer
- The vibration and nonlinear dynamic analysis
- Elastic foundation and temperature
- Analytical solutions, Hamilton's principle with the high-order shear deflection theory is used
- Galerkin method and the fourth-order Runge–Kutta method are applied

ARTICLE HISTORY

Received 20 June 2020
Accepted 8 September 2020

KEYWORDS

Analytical solutions; elastic foundations; mechanical and thermal loads; porous core layer; sandwich FG-CNTRC plate; the third-order shear deformation plate theory (TSDT); the vibration and nonlinear dynamic analysis)

1. Introduction

With the advantages of advanced functionally graded carbon nanotube-reinforced composite (FG-CNTRC) materials such as light, heat-resistant, scientists' interest in them has increased significantly over the past two decades through peer-reviewed and published articles with different methods and theories [1–5]. Over the past few years, carbon nanotubes with advanced mechanical properties such as hard, light, and high-temperature resistance has become one of the ingredients that enhances heat resistance, increasing the durability of composite materials. Lin et al. investigated aeroelastic characteristics and nonlinear response of FG-CNTRC panel considering the transient heat. Shen, Liew, Kiani and other authors [6–16] studied different modelings of FG-CNTRC plates and shells resting on elastic foundations under thermal and mechanical loads along with the influence geometrical parameter, imperfection, volume fraction CNTs by higher order shear theory. To evaluate the role of volume fraction and distribution of CNTs on the natural frequency of composite conical panels made of a polymeric matrix reinforced, the first order shear deformation shell theory (FSDT) and the Donnell's theory were used by Kiani [17]. Lei et al. [18] analyzed the free vibration

behaviors of functionally graded carbon nanotube (FG-CNT) reinforced composite thick straight-sided quadrilateral plates resting on Pasternak foundations by using IMLS-Ritz method. Zhang et al. [19] used Reddy's third-order shear deformation theory (HSDT), the Hamilton's principle and the state-space Levy method to obtain the results about the natural frequencies and vibration of FG-CNT reinforced composite plates subjected to in-plane loads. Qin et al. [20] combined the unified Fourier series with the first-order shear deformation theory (FSDT) in order to solve the vibration problem of FG-CNTRC cylindrical shells, conical shells and annular plates subjected to general boundary conditions. The used method in Qin's paper has been verified for its advantages, precision and convergence by numerical examples. Jiao et al. [21] considered the effect of five types of carbon nanotubes (CNTs) distribution on the dynamic buckling behavior of FG-CNTRC cylindrical shell under dynamic displacement load by using a semi-analytical. By the Budiansky–Roth criterion, the dynamic critical buckling condition of FG-CNTRC cylindrical shell is determined and compared with different published papers. Khoa ND et al. [22] researched the nonlinear dynamic response and vibration of FG-CNTs-reinforced composite cylindrical panels

with the support elastic foundations subjected to mechanical, thermal, and damping loads based on Reddy's higher order shear deformation shell theory.

In fact, the material manufacturing process has the appearance of micro holes in the surface as well as inside the material. This porosity factor directly affects the mechanical properties of the material such as Young modulus, density. Therefore, recently, there have been many studies focusing on investigating the effect of porosity on the static and dynamic response of structures such as Foroutan et al. [23] investigated the nonlinear dynamic and static hygrothermal buckling analysis of imperfect functionally graded porous (FGP) cylindrical shells under hygrothermal loading using the analytical and semi-analytical solutions. In order to find the nonlinear dynamic hygrothermal buckling responses, the fourth-order Runge–Kutta method is used. Due to the pore-network modeling needs much less computational resources, while still retaining essentials of the pore-structure information. So, a dynamic pore-network model of air–water flow with phase change has been developed with drainage processes through thin porous layers, in which liquid water is the nonwetting phase was studied by Qin et al. [24]. Jalaei and Thai [25] used Navier, Bolotin's methods along with quasi-3D sinusoidal shear deformation plate theory as well as nonlocal strain gradient theory (NSGT) to calculate the dynamic instability of viscoelastic porous functionally graded (FG) nanoplates under biaxial oscillating loading and longitudinal magnetic field. Metal tailings porous concrete (MTPC) not only holds good mechanical and physical properties but also reduces the environmental pollution caused by the disposal of waste metal tailings. Thus, Li et al. [26] systematically investigated the strain rate effect on the dynamic mechanical properties of MTPC. By using both Euler Bernoulli and Timoshenko beam theories as well as a finite element method (FEM), the free and forced vibration analyses of FGP beam type structures were analyzed by Wu et al. [27]. Jalaei et al. [28] presented dynamic instability of viscoelastic porous functionally graded (FG) nanobeam embedded on visco-Pasternak medium subjected to an axially oscillating loading as well as a magnetic field. In order to solve the problem and obtain the results, employing Eringen's differential law, Timoshenko beam theory (TBT) and Bolotin's method are approached. Chen et al. [29] focused on the analysis of dynamic response and energy absorption of closed-cell metal foams with different porosity distributions by using FEM. By using the Reddy's higher order shear deformation theory and Galerkin method, the buckling and post-buckling behavior of FG plates with the effect of porosity distribution characteristics (Porosity-I and Porosity-II) along with the influence of geometrical parameters, elastic foundations, material properties were investigated by Cong et al. [30]. In order to investigate the influence of porosity and temperature on the instabilities of porous FGM box beams, Ziane et al. [31] proposed an analytical method as well as Galerkin method and the commercial FEM code Abaqus to verify the accuracy of the obtained results. Demirhan and Taskin [32] studied the bending and free vibration of FG plate with the influence of porosity distribution on the property's material FG through the thickness of the structure by using Hamilton principle and State-space approach.

Besides single-layer materials, laminated FG-CNTRC material is attracting the attention of scientists in the world. Safaei et al. [33] considered the modeling which is made from one porous polymeric core and two carbon nanotube (CNT)/polymer nanocomposite outer layers under thermal gradient and mechanical loads. Eshelby–Mori–Tanaka's approach and a mesh-free method are used to observe thermoelastic static responses of Safaei's modeling and it indicated that the deflection of porous nanocomposite sandwich plates did not change significantly when adding 5% of CNTs volume fraction. Dynamic response of auxetic honeycomb plates integrated with agglomerated CNT-reinforced face sheets subjected to blast load based on visco-sinusoidal theory was proposed by Hajmohammad et al. [34]. Natarajan et al. [35] mentioned the application of the higher-order structural theory to bending and free vibration analysis of sandwich plates with CNT reinforced composite face sheets. Nonlinear vibration and bending of sandwich plates with nanotube-reinforced composite face sheets were investigated by Wang and Shen in [36]. Saidi et al. [37] presented the vibration and stability analysis of porous plates reinforced by graphene platelets under aerodynamic loading.

From literature review, the modeling which has not been proposed from previous studies: the sandwich plate is made by three layers in which the core layer is porous functionally graded material (FGM), bottom and top surfaces are FG-CNTRC. In order to achieve the set goals of this study as the effect of porosity and CNTs on the dynamic response and vibration of FG-CNTRC sandwich plates, analytical solutions, Reddy's third-order shear deformation plate theory and Galerkin method are used. The natural frequencies of the porous sandwich plate (PSP) are obtained by applying the fourth-order Runge–Kutta method. Moreover, the influence of geometrical parameters, temperature, elastic foundations and imperfections are indicated. The obtained results also indicated that porosity is a defect of the material and reduces material properties but it will be limited by the reinforcement of two layers of CNTs. Especially, in order to increase the reliability of using the analytical method, the obtained results are assessed by comparison with the results of other author's publications.

The other novelty of this work also is using the analytical method while other authors often used the FEM, so vibration frequencies and dynamic responses are expressed explicitly through the initial parameters and thus changing these parameters we can actively control the vibration and dynamic behaviors of the structures.

2. Modeling of the PSP with CNTRC face sheets

2.1. The configuration of modeling

The space coordinate system and geometrical configuration of modeling are shown in Figure 1a and b. Considering the modeling is made by three layers in which middle layers is the porous core, top and bottom are FGM is reinforced by CNTs with

a : length, b : width,

$h = h_c + 2h_f$: total thickness, core thickness and thickness of face layers respectively, k_1 is Winkler foundation modulus,

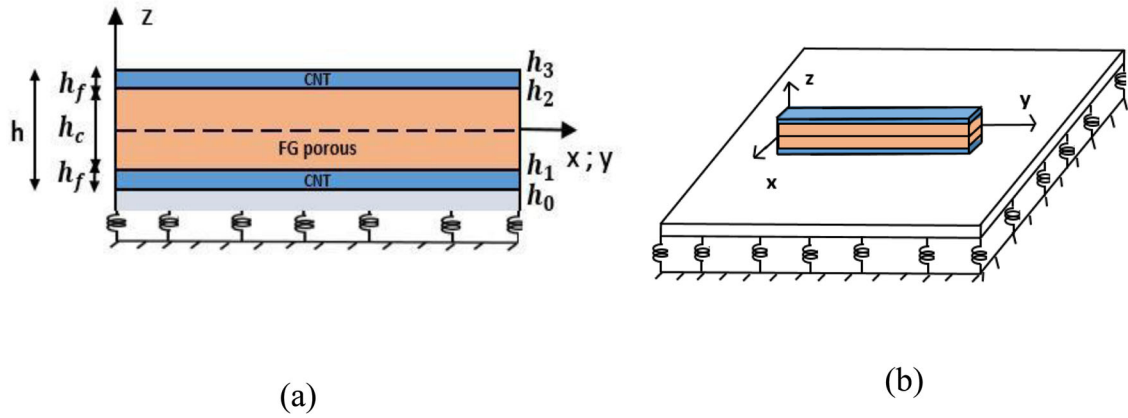


Figure 1. (a) PSP with three layers: FG-CNTRC bottom face sheet, core layers and top face sheet. (b) PSP resting on elastic foundations is placed on a space coordinate system (x, y, z) .

k_2 is the shear layer foundation stiffness of Pasternak model, u, v, w are displacement components corresponding to the coordinates (x, y, z) , ϕ_x, ϕ_y are the slopes of the transverse normal about the x and y axes at $z = 0$, respectively.

2.1.1. Porous core

Assume that the middle layer of the modeling is made by FGP material and it shows in Figure 2. The variation of elastic modulus, the density and thermal expansion coefficient through the thickness direction of the PSP are shown as [38]:

$$\begin{aligned} E^c &= E_1[1 - e_0\lambda(z)], \\ \rho^c &= \rho_1[1 - e_m\lambda(z)], \\ \alpha^c &= \alpha_1[1 - e_m\lambda(z)]. \end{aligned} \quad (1)$$

in which

$$\lambda(z) = \begin{cases} \lambda & \text{Uniform distribution} \\ \cos\left(\frac{\pi z}{h_c}\right) & \text{Non-uniform symmetric porosity distribution type 1} \\ \cos\left(\frac{\pi z}{2h_c} + \frac{\pi}{4}\right) & \text{Non-uniform asymmetric porosity distribution type 2} \end{cases}$$

e_0 and e_m denotes the coefficient of porosity and mass density and can determine as [38]:

$$\begin{aligned} e_0 &= 1 - \frac{E_2}{E_1} = 1 - \frac{G_2}{G_1}; \quad (0 \leq e_0 \leq 1), \\ e_m &= 1 - \sqrt{1 - e_0}. \end{aligned} \quad (2)$$

with G_1, G_2 is maximum and minimum value of shear's modulus for non-porosity distribution, $E_i (i = 1, 2)$ are the corresponding extremum values of elastic modulus.

In the case of uniform porosity distribution, the elastic modulus will be constant. In other words, the elastic modulus will not change according to the thickness of the core layer and will be determined by the following Eq. (3) and is shown in Figure 2a.

$$\lambda = \frac{1}{e_0} - \frac{1}{e_0} \left(\frac{2}{\pi} \sqrt{1 - e_0} - \frac{2}{\pi} + 1 \right)^2. \quad (3)$$

From Figure 2, it can be seen that the porous (type 1) will be distributed more on the two surfaces of the core layer and the porous will decrease when near the middle surface of the core layer (symmetrical through the x -axis). In other words, it can be described that the elastic modulus

reaches the highest value E_1 at the surface of the core layer and decreases with Eq. (2) and elastic modulus reaches the minimum value E_2 at the middle surface of the core layer. The distribution of the porosity type 2 is not the same as the distribution of the porosity type 1, the porosity type 2 will be distributed more on one surface and gradually reduced to the other surface according to Eq. (2). It can be described that the elastic modulus reaches the highest value E_1 at the surface of the core layer and reaches the minimum value E_2 at the other surface.

For the homogeneous core layer, the titanium alloy (Ti-6Al-4V) is chosen with the material properties are assumed to express as a nonlinear function of temperature expects for Position ratio and mass density.

$$\begin{aligned} \nu_1 &= 0.29, \rho_1 = 4429 \text{ kg/m}^3, E_1 = 122.56(1 - 4.586 \times 10^{-4}T) \text{ GPa}, \\ \alpha_1 &= 7.5788(1 + 6.638 \times 10^{-4}T + 3.147 \times 10^{-6}T^2) \times 10^{-6} / \text{K}. \end{aligned} \quad (4)$$

2.1.2. Face sheets

In this study, the face sheets (top face-sheet and bottom face-sheet) is an FG reinforced by nanocarbon tubes with the purpose of increasing the structural strength, called FG-CNTRC material. Currently, FG-CNTRC material is divided into five categories namely FG-O, FG-V, FG-X, UD and FG-A based on the distribution of nanotubes according to the thickness as shown in Figure 3. The distribution of nanocarbon tubes in the FG material is shown in Figure 4 and the volume change is shown in the equation below [39]:

FG-AV: top face-sheet is made by the FG-V type carbon nanotube-reinforced composite and bottom face-sheet is made by FG-A type carbon nanotube reinforced composite

$$V_{CNT}(z) = \begin{cases} \left(\frac{z - h_1}{h_0 - h_1}\right) 2V_{CNT}^* & \text{bottom face} \\ 0 & \text{middleface} \\ \left(\frac{h_2 - z}{h_2 - h_3}\right) 2V_{CNT}^* & \text{topface} \end{cases},$$

$$V_m(z) = 1 - V_{CNT}(z).$$

FG-OO: both face sheets are made by FG-O type carbon nanotube-reinforced composite

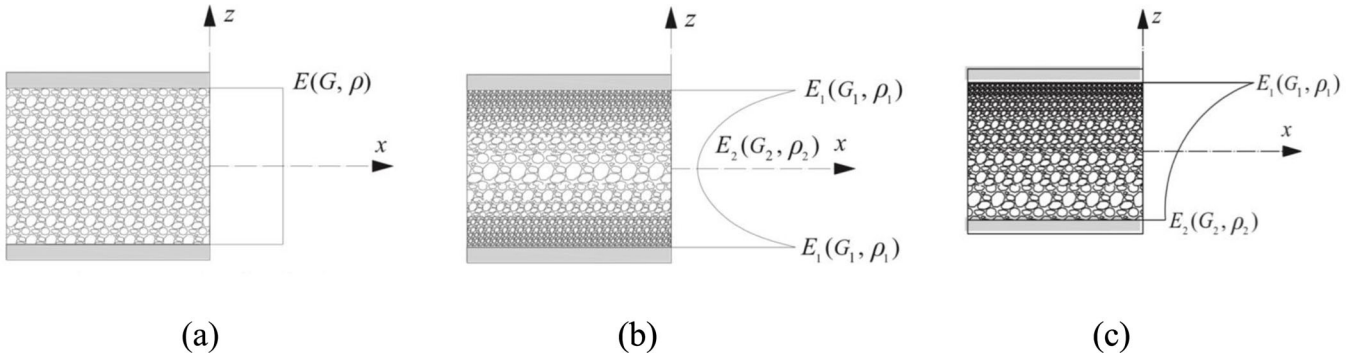


Figure 2. Different porosity distribution in porous cores.

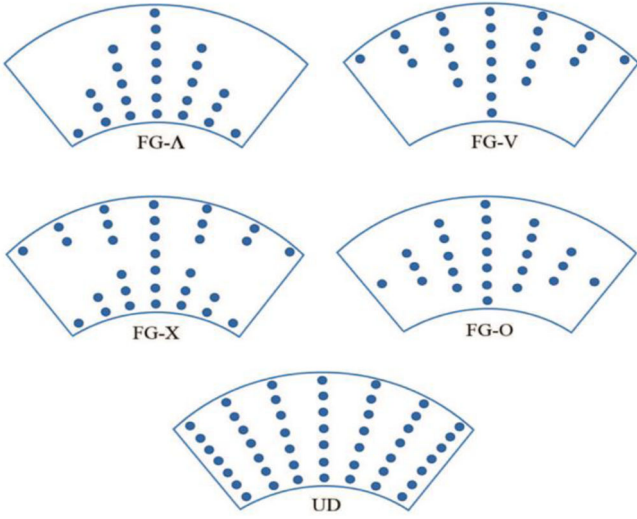


Figure 3. Configurations of CNTRCs: FG-A, FG-V, FG-X, FG-O and UD.

$$V_{CNT}(z) = \begin{cases} 2 \left(1 - \left| \frac{h_0 + h_1 - 2z}{h_0 - h_1} \right| \right) V_{CNT}^* & \text{bottom face} \\ 0 & \text{middle face} \\ 2 \left(1 - \left| \frac{h_3 + h_2 - 2z}{h_2 - h_3} \right| \right) V_{CNT}^* & \text{topface} \end{cases}$$

$$V_m(z) = 1 - V_{CNT}(z).$$

FG-XX: both face sheets is made by FG-X type carbon nanotube -reinforced composite

$$V_{CNT}(z) = \begin{cases} 2 \left(\left| \frac{h_0 + h_1 - 2z}{h_0 - h_1} \right| \right) V_{CNT}^* & \text{bottom face} \\ 0 & \text{middle face} \\ 2 \left(\left| \frac{h_2 + h_3 - 2z}{h_2 - h_3} \right| \right) V_{CNT}^* & \text{topface} \end{cases} \quad (5)$$

$$V_m(z) = 1 - V_{CNT}(z).$$

with

$$V_{CNT}^* = \frac{w_{CNT}}{-\frac{\rho_{CNT}}{\rho_m} w_{CNT} + w_{CNT} + (\rho_{CNT}/\rho_m)}. \quad (6)$$

in which w_{CNT} is the mass fraction of CNTs, ρ_{CNT} is the density of CNTs, ρ_m is the density of matrix.

According to Refs. [6–11], the properties of the FG-CNTRC material as Young's modulus and shear modulus dependent on Young's and shear modulus of the CNT

$E_{11}^{CNT}, E_{22}^{CNT}, G_{12}^{CNT}$, mechanical properties of the matrix E_m, G_m , the volume fractions of the CNT V_{CNT} and the volume matrix V_m and the CNT efficiency parameters $\eta_i (i = \overline{1, 3})$. It is determined as:

$$\begin{aligned} \eta_2/E_{22} &= V_{CNT}/E_{22}^{CNT} + V_m/E_m, \\ E_{11} &= \eta_1 V_{CNT} E_{11}^{CNT} + V_m E_m, \\ \eta_3/G_{12} &= V_{CNT}/G_{12}^{CNT} + V_m/G_m. \end{aligned} \quad (7)$$

The material properties of the matrix are determined as [6–11]:

$$\begin{aligned} \nu_m &= 0.34, E_m = (3.52 - 0.0034T) \text{GPa}, \\ \alpha_m &= 45(1 + 0.0005\Delta T) \times 10^{-6}/\text{K}. \end{aligned} \quad (8)$$

with $T = T_0 + \Delta T$, ΔT is the temperature increment in the environment and $T_0 = 300\text{K}$ (room temperature).

For the carbon nanotubes, the material properties of (10,10) SWCNTs as Elastic modulus $E_{11}^{CNT}, E_{22}^{CNT}$, Shear modulus G_{12}^{CNT} and $\alpha_{11}^{CNT}, \alpha_{22}^{CNT}$ thermal expansion coefficients are obtained with temperature change. According to Shen and Xiang [9], these properties at five certain temperature levels, i.e. $T = 300, 400, 500, 700, 1000$ are shown in Table 1 with $h = 0.067\text{m}$ and $\nu_{12}^{CNT} = 0.175$.

By matching the properties of FG-CNTRC material as the shear modulus G_{12} and Young's modulus E_{11} and E_{22} , the CNT efficiency parameters $\eta_i (i = \overline{1, 3})$ used in Eq. (7) are estimated. For three different volume fractions of CNTs, these parameters are determined in Table 2 [6–11].

The effective Poisson's ratio is defined as function on temperature change and position [6–11]:

$$\nu_{12} = V_{CNT}^* \nu_{12}^{CNT} + V_m \nu_m. \quad (9)$$

where ν_{12}^{CNT} is the Poisson's ratio of the CNT, ν_m is the Poisson's ratio of the matrix.

The thermal expansion coefficients in the longitudinal and transverse directions of the CNTRCs are expressed by Refs. [6–11]

$$\begin{aligned} \alpha_{11} &= \frac{E_{11}^{CNT} V_{CNT} \alpha_{11}^{CNT} + E_m V_m \alpha_m}{E_{11}^{CNT} V_{CNT} + E_m V_m}, \\ \alpha_{22} &= V_m \alpha (1 + \nu_m)_m + V_{CNT} \alpha_{22}^{CNT} (1 + \nu_{12}^{CNT}) - \nu_{12} \alpha_{11}. \end{aligned} \quad (10)$$

with $\alpha_{11}^{CNT}, \alpha_{22}^{CNT}$ is the thermal expansion coefficients of the CNT, α_m is the thermal expansion coefficients of the matrix.

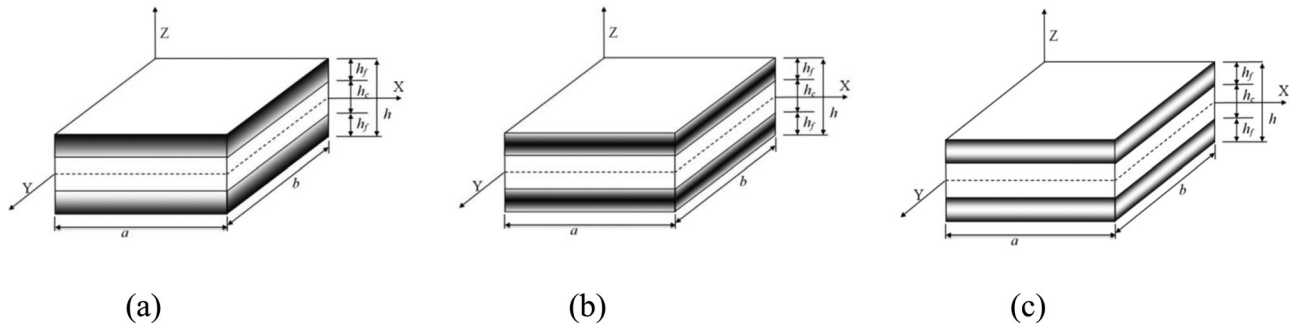


Figure 4. The face sheets are reinforced with various types of CNTs.

Table 1. Temperature-dependent material properties for (10, 10) SWCNTs.

T(K)	300	400	500	700	1000
$\alpha_{22}^{CNT} (\times 10^{-6}/K)$	5.1682	5.0905	5.0189	4.8943	4.7532
$\alpha_{11}^{CNT} (\times 10^{-6}/K)$	3.4584	4.1496	4.5361	4.5361	4.2800
E_{22}^{CNT} (TPa)	7.0800	6.9814	6.9348	6.8641	6.6220
G_{12}^{CNT} (TPa)	1.9445	1.9703	1.9643	1.9644	1.9451
E_{11}^{CNT} (TPa)	5.6466	5.5679	5.5308	5.4744	5.2814

Table 2. The CNT efficiency parameters for (10, 10).

V_{CNT}^*	Rule of mixture		
	η_1	η_2	η_3
0.12	0.137	1.022	0.715
0.17	0.142	1.626	1.138
0.28	0.141	1.585	1.109

2.2. Basic equations

In order to analyze the mechanical behavior of PSP with supported by elastic foundations under thermal load and mechanical load, Reddy's third-order shear deformation plate theory is proposed to use.

2.2.1. Displacements and strains

The displacement of PSP in three direction are (x, y, z) , respectively. In $z=0$ of PSP, ϕ_x, ϕ_y show angle of rotation about y and x , respectively. The normal strains are shown in Eq. (11) via displacements u, v, w and angle of rotation ϕ_x, ϕ_y according to Ref. [17]

$$\begin{bmatrix} \varepsilon_x^0 \\ \varepsilon_y^0 \\ \gamma_{xy}^0 \end{bmatrix} = \begin{bmatrix} \frac{\partial u}{\partial x} + \frac{1}{2} \left(\frac{\partial w}{\partial x} \right)^2 \\ \frac{\partial v}{\partial y} + \frac{1}{2} \left(\frac{\partial w}{\partial y} \right)^2 \\ \frac{\partial u}{\partial y} + \frac{\partial v}{\partial x} + \frac{\partial w}{\partial x} \frac{\partial w}{\partial y} \end{bmatrix}, \quad \begin{bmatrix} \gamma_{xz}^0 \\ \gamma_{yz}^0 \end{bmatrix} = -3c_1 \begin{bmatrix} \frac{\partial w}{\partial x} + \phi_x \\ \frac{\partial w}{\partial y} + \phi_y \end{bmatrix}. \quad (11)$$

According to von Karman nonlinear terms and Reddy's third order shear deformation plate theory (TSDT), the strain-displacement relations are given as [17]

$$\begin{bmatrix} \varepsilon_x \\ \varepsilon_y \\ \gamma_{xy} \end{bmatrix} = \begin{bmatrix} \varepsilon_x^0 \\ \varepsilon_y^0 \\ \gamma_{xy}^0 \end{bmatrix} + z \begin{bmatrix} k_x^1 \\ k_y^1 \\ k_{xy}^1 \end{bmatrix} + z^3 \begin{bmatrix} k_x^3 \\ k_y^3 \\ k_{xy}^3 \end{bmatrix}, \quad (12)$$

$$\begin{bmatrix} \gamma_{xz} \\ \gamma_{yz} \end{bmatrix} = \begin{bmatrix} \gamma_{xz}^0 \\ \gamma_{yz}^0 \end{bmatrix} + z^2 \begin{bmatrix} k_{xz}^2 \\ k_{yz}^2 \end{bmatrix}.$$

with

$$\begin{bmatrix} k_x^1 \\ k_y^1 \\ k_{xy}^1 \end{bmatrix} = \begin{bmatrix} \frac{\partial \phi_x}{\partial x} \\ \frac{\partial \phi_y}{\partial y} \\ \frac{\partial \phi_x}{\partial y} + \frac{\partial \phi_y}{\partial x} \end{bmatrix},$$

$$\begin{bmatrix} k_x^3 \\ k_y^3 \\ k_{xy}^3 \end{bmatrix} = -c_1 \begin{bmatrix} \frac{\partial \phi_x}{\partial x} + \frac{\partial^2 w}{\partial x^2} \\ \frac{\partial \phi_y}{\partial y} + \frac{\partial^2 w}{\partial y^2} \\ \frac{\partial \phi_x}{\partial y} + \frac{\partial \phi_y}{\partial x} + 2 \frac{\partial^2 w}{\partial x \partial y} \end{bmatrix}, \quad (13)$$

$$\begin{bmatrix} k_{xz}^2 \\ k_{yz}^2 \end{bmatrix} = -3c_1 \begin{bmatrix} \frac{\partial w}{\partial x} + \phi_x \\ \frac{\partial w}{\partial y} + \phi_y \end{bmatrix}.$$

2.2.2. Motion equations and Hook's law

The geometrical compatibility equation for an imperfect PSP is written as [17]

$$\varepsilon_{x,yy}^0 - \gamma_{xy,xy}^0 + \varepsilon_{y,xx}^0 = \frac{\partial^2 w^2}{\partial x \partial y} - w_{,xx}^2 w_{,yy}^2 + 2w_{,xy}^2 w_{,xy}^{*2} - \frac{\partial^2 w}{\partial x^2} \frac{\partial^2 w^*}{\partial y^2} - w_{,yy}^2 w_{,xx}^{*2}. \quad (14)$$

in which imperfection function $w^*(x, y)$ denotes initial small imperfection of PSP.

According to the Hooke's law, the relationships between stress and strain for the porous core take into account the effect of temperature are shown as [22]

$$\begin{bmatrix} \sigma_{xx} \\ \sigma_{yy} \\ \sigma_{xy} \\ \sigma_{xz} \\ \sigma_{yz} \end{bmatrix}_C = \begin{bmatrix} C_{11}^C & C_{12}^C & 0 & 0 & 0 \\ C_{12}^C & C_{22}^C & 0 & 0 & 0 \\ 0 & 0 & C_{66}^C & 0 & 0 \\ 0 & 0 & 0 & C_{44}^C & 0 \\ 0 & 0 & 0 & 0 & C_{55}^C \end{bmatrix} \begin{bmatrix} (\varepsilon_{xx})_C - \alpha_{11}\Delta T \\ (\varepsilon_{yy})_C - \alpha_{22}\Delta T \\ (\varepsilon_{xy})_C \\ (\varepsilon_{xz})_C \\ (\varepsilon_{yz})_C \end{bmatrix}. \quad (15a)$$

where

$$C_{11}^C = C_{22}^C = \frac{E^C}{1 - (\nu^C)^2}, C_{12}^C = \frac{\nu^C E^C}{1 - (\nu^C)^2}, \\ C_{66}^C = C_{44}^C = C_{55}^C = \frac{E^C}{2(1 + \nu^C)}.$$

The relationship stress and deformation of an FG-CNTRC with temperature-dependent properties are expressed through Hooke's law as [17]

$$\begin{bmatrix} \sigma_{xx} \\ \sigma_{yy} \\ \sigma_{xy} \\ \sigma_{xz} \\ \sigma_{yz} \end{bmatrix}_f = \begin{bmatrix} C_{11} & C_{12} & 0 & 0 & 0 \\ C_{12} & C_{22} & 0 & 0 & 0 \\ 0 & 0 & C_{66} & 0 & 0 \\ 0 & 0 & 0 & C_{44} & 0 \\ 0 & 0 & 0 & 0 & C_{55} \end{bmatrix}_f \begin{bmatrix} (\varepsilon_{xx})_f - \alpha_{11}\Delta T \\ (\varepsilon_{yy})_f - \alpha_{22}\Delta T \\ (\varepsilon_{xy})_f \\ (\varepsilon_{xz})_f \\ (\varepsilon_{yz})_f \end{bmatrix}. \quad (15b)$$

where

$$C_{12} = \frac{\nu_{21}E_{11}}{1 - \nu_{12}\nu_{21}} C_{11} = \frac{E_{11}}{1 - \nu_{12}\nu_{21}}, C_{44} = G_{12}, \\ C_{44} = G_{23}, C_{55} = G_{13}, C_{22} = \frac{E_{22}}{1 - \nu_{12}\nu_{21}}.$$

and we assume that $G_{13} = G_{12}$ and $G_{23} = 1.2G_{12}$.

The force and moment resultants of PSP are expressed by

$$(N_i, M_i, P_i) = \int_{-\frac{h_2}{2}}^{\frac{h_2}{2}} \sigma_i^f(1, z, z^3) dz + \int_{-\frac{h_2}{2}}^{\frac{h_2}{2}} \sigma_i^C(1, z, z^3) dz \\ + \int_{\frac{h_2}{2}+h_1}^{\frac{h_2}{2}} \sigma_i^f(1, z, z^3) dz, i = x, y, xy, \quad (16) \\ (Q_i, R_i) = \int_{-\frac{h_2}{2}-h_3}^{\frac{h_2}{2}} \sigma_{iz}^f(1, z^2) dz + \int_{-\frac{h_2}{2}}^{\frac{h_2}{2}} \sigma_{iz}^C(1, z^2) dz \\ + \int_{\frac{h_2}{2}+h_1}^{\frac{h_2}{2}} \sigma_{iz}^f(1, z^2) dz, i = x, y.$$

The nonlinear equations of motion for the PSP are [17]

$$\frac{\partial N_x}{\partial x} + \frac{\partial N_{xy}}{\partial y} = \bar{\Lambda}_1 \frac{\partial^2 u}{\partial t^2} + \bar{\Lambda}_2 \frac{\partial^2 \phi_x}{\partial t^2} - \bar{\Lambda}_3 \frac{\partial^3 w}{\partial t^2 \partial x}, \quad (17a)$$

$$\frac{\partial N_{xy}}{\partial x} + \frac{\partial N_y}{\partial y} = \bar{\Lambda}_1^* \frac{\partial^2 v}{\partial t^2} + \bar{\Lambda}_2^* \frac{\partial^2 \phi_y}{\partial t^2} - \bar{\Lambda}_3^* \frac{\partial^3 w}{\partial t^2 \partial y}, \quad (17b)$$

$$\frac{\partial Q_x}{\partial x} + \frac{\partial Q_y}{\partial y} - 3c_1 \left(\frac{\partial R_x}{\partial x} + \frac{\partial R_y}{\partial y} \right) + c_1 \left(\frac{\partial^2 P_x}{\partial x^2} + 2 \frac{\partial^2 P_y}{\partial x \partial y} + \frac{\partial^2 P_y}{\partial y^2} \right) \\ + \frac{N_x}{R_x} + \frac{N_y}{R_y} + q + N_x \frac{\partial^2 w}{\partial x^2} \\ + 2N_{xy} \frac{\partial^2 w}{\partial x \partial y} + N_y \frac{\partial^2 w}{\partial y^2} - k_1 w + k_2 \nabla^2 w \\ = \bar{\Lambda}_1 \frac{\partial^2 w}{\partial t^2} + 2\varepsilon \bar{\Lambda}_1 \frac{\partial w}{\partial t} + \bar{\Lambda}_3 \frac{\partial^3 u}{\partial t^2 \partial x} + \bar{\Lambda}_5 \frac{\partial^3 \phi_x}{\partial t^2 \partial x} \\ + \bar{\Lambda}_3^* \frac{\partial^3 v}{\partial t^2 \partial y} + \bar{\Lambda}_5^* \frac{\partial^3 \phi_y}{\partial t^2 \partial y} - c_1^2 \bar{\Lambda}_7 \left(\frac{\partial^4 w}{\partial t^2 \partial x^2} + \frac{\partial^4 w}{\partial t^2 \partial y^2} \right), \quad (17c)$$

$$\frac{\partial M_x}{\partial x} + \frac{\partial M_{xy}}{\partial y} - Q_x + 3c_1 R_x - c_1 \left(\frac{\partial P_x}{\partial x} + \frac{\partial P_{xy}}{\partial y} \right) \\ = \bar{\Lambda}_2 \frac{\partial^2 u}{\partial t^2} + \bar{\Lambda}_4 \frac{\partial^2 \phi_x}{\partial t^2} - \bar{\Lambda}_5 \frac{\partial^3 w}{\partial t^2 \partial x}, \quad (17d)$$

$$\frac{\partial M_{xy}}{\partial x} + \frac{\partial M_y}{\partial y} - Q_y + 3c_1 R_y - c_1 \left(\frac{\partial P_{xy}}{\partial x} + \frac{\partial P_y}{\partial y} \right) \\ = \bar{\Lambda}_2^* \frac{\partial^2 v}{\partial t^2} + \bar{\Lambda}_4^* \frac{\partial^2 \phi_y}{\partial t^2} - \bar{\Lambda}_5^* \frac{\partial^3 w}{\partial t^2 \partial y}. \quad (17e)$$

in which ε is the viscous damping coefficient and

$$(\bar{\Lambda}_1, \bar{\Lambda}_2, \bar{\Lambda}_3, \bar{\Lambda}_4, \bar{\Lambda}_5, \bar{\Lambda}_7)$$

$$= \int_{-hf-hc/2}^{-hc/2} \rho_f(z)(1, z, z^2, z^3, z^4, z^6) dz \\ + \int_{-hc/2}^{hc/2} \rho_c(z)(1, z, z^2, z^3, z^4, z^6) dz \\ + \int_{hc/2}^{hc/2+hf} \rho_f(z)(1, z, z^2, z^3, z^4, z^6) dz, \quad (18)$$

$$\bar{\Lambda}_1 = \bar{\Lambda}_1, \bar{\Lambda}_2 = \bar{\Lambda}_2 - c_1 \bar{\Lambda}_4, \bar{\Lambda}_3 = c_1 \bar{\Lambda}_4, \\ \bar{\Lambda}_4 = \bar{\Lambda}_3 - 2c_1 \bar{\Lambda}_5 + c_1^2 \bar{\Lambda}_7, \bar{\Lambda}_5 = c_1 \bar{\Lambda}_5 - c_1^2 \bar{\Lambda}_7.$$

Substitution of Eqs. (12) into Eqs. (15) and the result into Eqs. (16) yields the constitutive relations as

$$N_x = T_{11}\varepsilon_x^0 + T_{12}\varepsilon_y^0 + H_{11}k_x^1 + H_{12}k_y^1 + L_{11}k_x^3 + L_{12}k_y^3 - \Phi_1, \\ N_y = T_{12}\varepsilon_x^0 + T_{22}\varepsilon_y^0 + H_{12}k_x^1 + H_{22}k_y^1 + L_{12}k_x^3 + L_{22}k_y^3 - \Phi_2, \\ N_{xy} = T_{66}\gamma_{xy}^0 + H_{66}k_{xy}^1 + L_{66}k_{xy}^3, \\ M_x = H_{11}\varepsilon_x^0 + H_{12}\varepsilon_y^0 + K_{11}k_x^1 + K_{12}k_y^1 + Y_{11}k_x^3 + Y_{12}k_y^3 - \Phi_3,$$

$$\begin{aligned}
M_y &= H_{12}\varepsilon_x^0 + H_{22}\varepsilon_y^0 + K_{12}k_x^1 + K_{22}k_y^1 + Y_{12}k_x^3 + Y_{22}k_y^3 - \Phi_4, \\
M_{xy} &= H_{66}\gamma_{xy}^0 + K_{66}k_{xy}^1 + Y_{66}k_{xy}^3, \\
P_x &= L_{11}\varepsilon_x^0 + L_{12}\varepsilon_y^0 + Y_{11}k_x^1 + Y_{12}k_y^1 + O_{11}k_x^3 + O_{12}k_y^3 - \Phi_5, \\
P_y &= L_{12}\varepsilon_x^0 + L_{22}\varepsilon_y^0 + Y_{12}k_x^1 + Y_{22}k_y^1 + O_{12}k_x^3 + O_{22}k_y^3 - \Phi_6, \\
P_{xy} &= L_{66}\gamma_{xy}^0 + Y_{66}k_{xy}^1 + O_{66}k_{xy}^3, \\
Q_x &= T_{44}\gamma_{xz}^0 + K_{44}k_{xz}^2, \quad Q_y = T_{55}\gamma_{yz}^0 + K_{55}k_{yz}^2, \\
R_x &= D_{44}\gamma_{xz}^0 + F_{44}k_{xz}^2, \quad R_y = D_{55}\gamma_{yz}^0 + F_{55}k_{yz}^2,
\end{aligned} \tag{19}$$

in which

$$\begin{aligned}
(T_{kl}, D_{kl}, F_{kl}) &= \int_{-h_f-h_c/2}^{-h_c/2} C_{ij}(1, z^2, z^4) dz + \int_{-h_c/2}^{h_c/2} C_{ij}(1, z^2, z^4) dz \\
&+ \int_{h_c/2}^{h_c/2+h_f} C_{ij}(1, z^2, z^4) dz, \quad kl = 44, 55,
\end{aligned}$$

$$\begin{aligned}
&(T_{ij}, H_{ij}, K_{ij}, L_{ij}, Y_{ij}, O_{ij}) \\
&= \int_{-h_f-h_c/2}^{-h_c/2} C_{ij}(1, z, z^2, z^3, z^4, z^6) dz \\
&+ \int_{-h_c/2}^{h_c/2} C_{ij}(1, z, z^2, z^3, z^4, z^6) dz \\
&+ \int_{h_c/2}^{h_c/2+h_f} C_{ij}(1, z, z^2, z^3, z^4, z^6) dz, \quad ij = 11, 12, 22, 66,
\end{aligned}$$

$$\begin{aligned}
\Phi_1 &= \int_{-h_f-h_c/2}^{-h_c/2} C_{11}\alpha_{11}\Delta T dz + \int_{-h_f-h_c/2}^{-h_c/2} C_{12}\alpha_{22}\Delta T dz \\
&+ \int_{-h_c/2}^{h_c/2} C_{11}\alpha_{11}\Delta T dz + \int_{-h_c/2}^{h_c/2} C_{12}\alpha_{22}\Delta T dz \\
&+ \int_{h_c/2}^{h_f+h_c/2} C_{11}\alpha_{11}\Delta T dz + \int_{h_c/2}^{h_f+h_c/2} C_{12}\alpha_{22}\Delta T dz, \\
\Phi_2 &= \int_{-h_f-h_c/2}^{-h_c/2} C_{12}\alpha_{11}\Delta T dz + \int_{-h_f-h_c/2}^{-h_c/2} C_{22}\alpha_{22}\Delta T dz \\
&+ \int_{-h_c/2}^{h_c/2} C_{12}\alpha_{11}\Delta T dz + \int_{-h_c/2}^{h_c/2} C_{22}\alpha_{22}\Delta T dz \\
&+ \int_{h_c/2}^{h_f+h_c/2} C_{12}\alpha_{11}\Delta T dz + \int_{h_c/2}^{h_f+h_c/2} C_{22}\alpha_{22}\Delta T dz.
\end{aligned}$$

$$\begin{aligned}
\Phi_3 &= \int_{-h_f-h_c/2}^{-h_c/2} C_{11}\alpha_{11}z\Delta T dz + \int_{-h_f-h_c/2}^{-h_c/2} C_{12}\alpha_{22}z\Delta T dz \\
&+ \int_{-h_c/2}^{h_c/2} C_{11}\alpha_{11}z\Delta T dz + \int_{-h_c/2}^{h_c/2} C_{12}\alpha_{22}z\Delta T dz \\
&+ \int_{h_c/2}^{h_f+h_c/2} C_{11}\alpha_{11}z\Delta T dz + \int_{h_c/2}^{h_f+h_c/2} C_{12}\alpha_{22}z\Delta T dz, \\
\Phi_4 &= \int_{-h_f-h_c/2}^{-h_c/2} C_{12}\alpha_{11}z\Delta T dz + \int_{-h_f-h_c/2}^{-h_c/2} C_{22}\alpha_{22}z\Delta T dz \\
&+ \int_{-h_c/2}^{h_c/2} C_{12}\alpha_{11}z\Delta T dz + \int_{-h_c/2}^{h_c/2} C_{22}\alpha_{22}z\Delta T dz \\
&+ \int_{h_c/2}^{h_f+h_c/2} C_{12}\alpha_{11}z\Delta T dz + \int_{h_c/2}^{h_f+h_c/2} C_{22}\alpha_{22}z\Delta T dz, \\
\Phi_5 &= \int_{-h_f-h_c/2}^{-h_c/2} C_{11}\alpha_{11}z^3\Delta T dz + \int_{-h_f-h_c/2}^{-h_c/2} C_{12}\alpha_{22}z^3\Delta T dz \\
&+ \int_{-h_c/2}^{h_c/2} C_{11}\alpha_{11}z^3\Delta T dz + \int_{-h_c/2}^{h_c/2} C_{12}\alpha_{22}z^3\Delta T dz \\
&+ \int_{h_c/2}^{h_f+h_c/2} C_{11}\alpha_{11}z^3\Delta T dz + \int_{h_c/2}^{h_f+h_c/2} C_{12}\alpha_{22}z^3\Delta T dz, \\
\Phi_6 &= \int_{-h_f-h_c/2}^{-h_c/2} C_{12}\alpha_{11}z^3\Delta T dz + \int_{-h_f-h_c/2}^{-h_c/2} C_{22}\alpha_{22}z^3\Delta T dz \\
&+ \int_{-h_c/2}^{h_c/2} C_{12}\alpha_{11}z^3\Delta T dz + \int_{-h_c/2}^{h_c/2} C_{22}\alpha_{22}z^3\Delta T dz \\
&+ \int_{h_c/2}^{h_f+h_c/2} C_{12}\alpha_{11}z^3\Delta T dz + \int_{h_c/2}^{h_f+h_c/2} C_{22}\alpha_{22}z^3\Delta T dz.
\end{aligned} \tag{20}$$

2.2.3. Conversion equation

The Airy's stress function $\psi(x, y, t)$ is defined as [22]

$$N_x = \psi_{,yy}, N_y = \psi_{,xx}, N_{xy} = -\psi_{,xy}. \tag{21}$$

From the constitutive relations (20) with Eq. (21), one can write:

$$\begin{aligned}
\varepsilon_x^0 &= \Lambda_{11}\psi_{,xx} - \Lambda_{12}\psi_{,xx} + \Lambda_{13}\phi_{x,xx} + \Lambda_{14}\phi_{y,xx} - c_1\Lambda_{15}(w_{,xx} + \phi_{x,xx}) \\
&\quad - c_1\Lambda_{16}(w_{,y} + \phi_{y,y}) + \Lambda_{17}\Phi_1 + \Lambda_{18}\Phi_2, \\
\varepsilon_y^0 &= \Lambda_{21}\psi_{,xx} - \Lambda_{12}\psi_{,yy} + \Lambda_{23}\phi_{x,x} + \Lambda_{24}\phi_{y,y} - c_1\Lambda_{25}(w_{,xx} + \phi_{x,x}) \\
&\quad - c_1\Lambda_{26}(w_{,yy} + \phi_{y,y}) + \Lambda_{27}\Phi_1 + \Lambda_{28}\Phi_2, \\
\gamma_{xy}^0 &= -\Lambda_{31}\psi_{,xy} + \Lambda_{32}(\phi_{x,y} + \phi_{y,x}) - c_1\Lambda_{33}(2w_{,xy} + \phi_{x,y} + \phi_{y,x}).
\end{aligned} \tag{22}$$

with

$$\begin{aligned}
\Delta &= T_{11}T_{22} - T_{12}^2, \Lambda_{11} = \frac{T_{22}}{\Delta}, \Lambda_{12} = \frac{T_{12}}{\Delta}, \\
\Lambda_{13} &= \frac{H_{12}T_{12} - H_{11}T_{22}}{\Delta}, \\
\Lambda_{14} &= \frac{H_{22}T_{12} - H_{12}T_{22}}{\Delta}, \Lambda_{15} = \frac{L_{12}T_{12} - L_{11}T_{22}}{\Delta}, \\
\Lambda_{16} &= \frac{L_{22}T_{12} - L_{12}T_{22}}{\Delta}, \\
\Lambda_{17} &= \frac{T_{22}}{\Delta}, \Lambda_{18} = -\frac{T_{12}}{\Delta}, \Lambda_{21} = \frac{T_{11}}{\Delta}, \\
\Lambda_{23} &= \frac{H_{11}T_{12} - H_{12}T_{11}}{\Delta}, \Lambda_{24} = \frac{H_{12}T_{12} - H_{22}T_{11}}{\Delta}, \\
\Lambda_{25} &= \frac{L_{11}T_{12} - L_{12}T_{11}}{\Delta}, \Lambda_{26} = \frac{L_{12}T_{12} - L_{22}T_{11}}{\Delta}, \\
\Lambda_{27} &= -\frac{T_{12}}{\Delta}, \Lambda_{28} = \frac{T_{11}}{\Delta}, \\
\Lambda_{31} &= \frac{1}{T_{66}}, \Lambda_{32} = -\frac{H_{66}}{T_{66}}, \Lambda_{33} = -\frac{L_{66}}{T_{66}}.
\end{aligned} \tag{23}$$

Imposing Eq. (21) into Eqs. (17a) and (17b) yields

$$\frac{\partial^2 u}{\partial t^2} = -\frac{\overline{\Lambda}_2}{\overline{\Lambda}_1}\phi_{x,tt} + \frac{\overline{\Lambda}_3}{\overline{\Lambda}_1}w_{,ttx}, \tag{24a}$$

$$\frac{\partial^2 v}{\partial t^2} = -\frac{\overline{\Lambda}_2^*}{\overline{\Lambda}_1^*}\phi_{y,tt} + \frac{\overline{\Lambda}_3^*}{\overline{\Lambda}_1^*}w_{,tty}. \tag{24b}$$

By substituting Eqs. (24a) and (24b) into Eqs. (17c)–(17e) leads to

$$\begin{aligned}
\frac{\partial M_x}{\partial x} + \frac{\partial M_{xy}}{\partial y} - Q_x + 3c_1R_x - c_1\left(\frac{\partial P_x}{\partial x} + \frac{\partial P_{xy}}{\partial y}\right) \\
= \overline{\overline{\Lambda}}_3\frac{\partial^2\phi_x}{\partial t^2} - \overline{\overline{\Lambda}}_5\frac{\partial^3 w}{\partial t^2\partial x},
\end{aligned} \tag{25a}$$

$$\begin{aligned}
\frac{\partial Q_x}{\partial x} + \frac{\partial Q_y}{\partial y} - 3c_1\left(\frac{\partial R_x}{\partial x} + \frac{\partial R_y}{\partial y}\right) \\
+ c_1\left(\frac{\partial^2 P_x}{\partial x^2} + 2\frac{\partial^2 P_{xy}}{\partial x\partial y} + \frac{\partial^2 P_y}{\partial y^2}\right) + \psi_{,yy}\frac{\partial^2 w}{\partial x^2} \\
- 2\psi_{,xy}\frac{\partial^2 w}{\partial x\partial y} + \psi_{,xx}\frac{\partial^2 w}{\partial y^2} + q - k_1w + k_2\nabla^2 w \\
= \Lambda_1\frac{\partial^2 w}{\partial t^2} + 2\varepsilon\Lambda_1\frac{\partial w}{\partial t} + \overline{\overline{\Lambda}}_5\frac{\partial^3\phi_x}{\partial t^2\partial x} + \overline{\overline{\Lambda}}_5^*\frac{\partial^3\phi_y}{\partial t^2\partial y} \\
+ \overline{\overline{\Lambda}}_7\frac{\partial^4 w}{\partial t^2\partial x^2} + \overline{\overline{\Lambda}}_7^*\frac{\partial^4 w}{\partial t^2\partial y^2},
\end{aligned} \tag{25b}$$

$$\begin{aligned}
\frac{\partial M_{xy}}{\partial x} + \frac{\partial M_y}{\partial y} - Q_y + 3c_1R_y - c_1\left(\frac{\partial P_{xy}}{\partial x} + \frac{\partial P_y}{\partial y}\right) \\
= \overline{\overline{\Lambda}}_3^*\frac{\partial^2\phi_y}{\partial t^2} - \overline{\overline{\Lambda}}_5^*\frac{\partial^3 w}{\partial t^2\partial y}.
\end{aligned} \tag{25c}$$

in which

$$\begin{aligned}
\overline{\overline{\Lambda}}_3 &= \overline{\Lambda}_4 - (\overline{\Lambda}_2)^2/\overline{\Lambda}_1, \overline{\overline{\Lambda}}_3^* = \overline{\Lambda}_4^* - (\overline{\Lambda}_2^*)^2/\overline{\Lambda}_1^*, \\
\overline{\overline{\Lambda}}_5 &= \overline{\Lambda}_5 - \overline{\Lambda}_2\overline{\Lambda}_3/\overline{\Lambda}_1, \\
\overline{\overline{\Lambda}}_5^* &= \overline{\Lambda}_5^* - \overline{\Lambda}_2^*\overline{\Lambda}_3^*/\overline{\Lambda}_1^*, \overline{\overline{\Lambda}}_7 = (\overline{\Lambda}_3)^2/\overline{\Lambda}_1 - c_1^2\Lambda_7, \\
\overline{\overline{\Lambda}}_7^* &= (\overline{\Lambda}_3^*)^2/\overline{\Lambda}_1^* - c_1^2\Lambda_7
\end{aligned} \tag{26}$$

Inserting Eqs. (11), (12) into Eq. (19) and then into Eqs. (25) gives

$$\begin{aligned}
SA_{11}(w) + SA_{12}(\phi_x) + SA_{13}(\phi_y) + SA_{14}(\psi) \\
+ SA(w, \psi) + q = \Lambda_1 w_{,tt} + 2\varepsilon\Lambda_1 w_{,t} \\
+ \overline{\overline{\Lambda}}_5\phi_{x,ttx} + \overline{\overline{\Lambda}}_5^*\phi_{y,tty} + \overline{\overline{\Lambda}}_7 w_{,ttxx} + \overline{\overline{\Lambda}}_7^* w_{,ttyy}, \\
SA_{21}(w) + SA_{22}(\phi_x) + SA_{23}(\phi_y) \\
+ SA_{24}(\psi) = \overline{\overline{\Lambda}}_3\phi_{x,tt} - \overline{\overline{\Lambda}}_5 w_{,ttx}, \\
SA_{31}(w) + SA_{32}(\phi_x) + SA_{33}(\phi_y) \\
+ SA_{34}(\psi) = \overline{\overline{\Lambda}}_3^*\phi_{y,tt} - \overline{\overline{\Lambda}}_5^* w_{,tty}.
\end{aligned} \tag{27}$$

in which linear parameters $SA_{ij}(i = \overline{1,3}; j = \overline{1,4})$, SA and the detail of coefficients $TB_{1i}(i = \overline{1,12})$, $TB_{2j}(j = \overline{1,8})$, $TB_{3k}(k = \overline{1,8})$ are defined in Appendix A.

For an imperfect PSP, Eqs. (27) may be transformed to the form as

$$\begin{aligned}
SA_{11}(w) + SA_{12}(\phi_x) + SA_{13}(\phi_y) + SA_{14}(\psi) \\
+ SA(w, \psi) + SA_{11}^*(w^*) + SA^*(w^*, \psi) \\
+ q = \Lambda_1 w_{,tt} + 2\varepsilon\Lambda_1 w_{,t} + \overline{\overline{\Lambda}}_5\phi_{x,ttx} \\
+ \overline{\overline{\Lambda}}_5^*\phi_{y,tty} + \overline{\overline{\Lambda}}_7 w_{,ttxx} + \overline{\overline{\Lambda}}_7^* w_{,ttyy}, \\
SA_{21}(w) + SA_{22}(\phi_x) + SA_{23}(\phi_y) + SA_{24}(\psi) \\
+ SA_{21}^*(w^*) = \overline{\overline{\Lambda}}_3\phi_{x,tt} - \overline{\overline{\Lambda}}_5 w_{,ttx}, \\
SA_{31}(w) + SA_{32}(\phi_x) + SA_{33}(\phi_y) + SA_{34}(\psi) \\
+ S_{31}^*(w^*) = \overline{\overline{\Lambda}}_3^*\phi_{y,tt} - \overline{\overline{\Lambda}}_5^* w_{,tty}.
\end{aligned} \tag{28}$$

in which

$$\begin{aligned}
SA_{11}^*(w^*) &= TB_{11}w_{,xx}^* + TB_{12}w_{,yy}^*, \\
SA^*(w^*, \psi) &= \psi_{,yy}w_{,xx}^* - 2\psi_{,xy}w_{,xy}^* + \psi_{,xx}w_{,yy}^*, \\
SA_{21}^*(w^*) &= TB_{21}w_{,x}^*, SA_{31}^*(w^*) = T_{31}w_{,y}^*.
\end{aligned} \tag{29}$$

Introduction of Eqs. (22) into Eq. (14) gives the compatibility equation of the imperfect PSP as

$$\begin{aligned} & \Lambda_{21}\psi_{,xxxx} + \Lambda_{11}\psi_{,yyyy} + V_1\psi_{,xxyy} + V_2\phi_{x,xxx} + V_3\phi_{x,xyy} + V_4\phi_{y,yyy} \\ & + V_5\phi_{y,xxx} - c_1\Lambda_{25}w_{,xxxx} - c_1\Lambda_{16}w_{,yyyy} + J_6w_{,xxyy} \\ & - \left(\frac{\partial^2 w^2}{\partial x \partial y} + 2 \frac{\partial^2 w}{\partial x \partial y} \frac{\partial^2 w^*}{\partial x \partial y} - \frac{\partial^2 w \partial^2 w}{\partial x^2 \partial y^2} - \frac{\partial^2 w \partial^2 w^*}{\partial x^2 \partial y^2} - \frac{\partial^2 w \partial^2 w^*}{\partial y^2 \partial x^2} \right) = 0. \end{aligned} \quad (30)$$

where

$$\begin{aligned} V_1 &= -2\Lambda_{12} + \Lambda_{31}, V_2 = -c_1\Lambda_{25} + \Lambda_{23}, \\ V_6 &= 2c_1\Lambda_{33} - c_1\Lambda_{15} - c_1\Lambda_{26}, \\ V_4 &= -c_1\Lambda_{16} + \Lambda_{14}, V_5 = c_1\Lambda_{33} + \Lambda_{24} - c_1\Lambda_{26} - \Lambda_{32}, \\ V_3 &= c_1\Lambda_{33} + \Lambda_{13} - c_1\Lambda_{15} - \Lambda_{32}. \end{aligned} \quad (31)$$

In order to research vibration and dynamic response of imperfect PSP, nonlinear Eqs. (28) and (30) are used with w, ϕ_x, ϕ_y and ψ are variables.

2.3. Nonlinear dynamic response

2.3.1. Boundary conditions

The four edges of imperfect PSP are assumed to be immovable and simply supported. Thus, the boundary conditions are determined as [22]

$$\begin{aligned} \begin{Bmatrix} \phi_x(x, y, t) \\ w(x, y, t) \\ \phi_y(x, y, t) \end{Bmatrix} &= \begin{bmatrix} \Phi_x(t) & 0 & 0 \\ 0 & W(t) & 0 \\ 0 & 0 & \Phi_y(t) \end{bmatrix} \\ &\times \begin{Bmatrix} \cos \lambda_m x \sin \delta_n y \\ \sin \lambda_m x \sin \delta_n y \\ \sin \lambda_m x \cos \delta_n y \end{Bmatrix}. \end{aligned} \quad (32)$$

in which $\lambda_m = m\pi/a, \delta_n = n\pi/b$, and m, n are mode of the buckling; Φ_x, Φ_y are amplitude of the angel of rotation; W is amplitude of the defection. In this assumption, the initial geometry imperfection w^* is introduced, it is defined same as form of deflection, i.e.

$$w^*(x, y, t) = W_0 \sin \lambda_m x \sin \delta_n y. \quad (33)$$

where $W_0 = \mu h$ is amplitude of the small imperfect function, and $0 \leq \mu \leq 1$ is imperfection parameter.

Replacing Eqs. (32), (33) into Eq. (30) and solving obtained equation for stress function $\psi(x, y, t)$ leads to:

$$\begin{aligned} \psi(x, y, t) &= X_1(t) \cos 2\lambda_m x + X_2(t) \cos 2\delta_n y \\ &+ X_3(t) \sin \lambda_m x \sin \delta_n y + \frac{1}{2} N_{y0} x^2 + \frac{1}{2} N_{x0} y^2. \end{aligned} \quad (34)$$

with

$$X_1 = \frac{\delta_n^2}{32I_{21}\lambda_m^2} W(W + 2\mu h), X_2 = \frac{\lambda_m^2}{32I_{11}\delta_n^2} W(W + 2\mu h), \quad (35)$$

$$X_3 = F_1 W + F_2 \Phi_x + F_3 \Phi_y. \quad (35)$$

and

$$\begin{aligned} F_1 &= \frac{c_1\Lambda_{25}\lambda_m^4 + c_1\Lambda_{16}\delta_n^4 - V_6\lambda_m^2\delta_n^2}{\Pi}, \\ F_2 &= \frac{-(V_2\lambda_m^3 + V_3\lambda_m\delta_n^2)}{\Pi}, F_3 = \frac{-(V_4\delta_n^3 + V_5\lambda_m^2\delta_n)}{\Pi}, \\ \Pi &= \Lambda_{21}\lambda_m^4 + V_1\lambda_m^2\delta_n^2 + \Lambda_{11}\delta_n^4. \end{aligned} \quad (36)$$

Replacing Eqs. (32–34) into Eq. (28) and then applying Galerkin method to the resulting equation yields

$$\begin{aligned} & sa_{11}W + sa_{12}\Phi_x + sa_{13}\Phi_y + sa_{14}(W + \mu h)\Phi_x + sa_{15}(W + \mu h)\Phi_y \\ & + [y_1 - N_{x0}\lambda_m^2 - N_{y0}\delta_n^2](W + \mu h) + y_2W(W + \mu h) \\ & + y_3W(W + 2\mu h) + y_4W(W + \mu h)(W + 2\mu h) \\ & + y_5q = \Lambda_0 W_{,tt} + 2\varepsilon\Lambda_1 W_{,t} - \lambda_m \overline{\Lambda_5} \frac{\partial^2 \Phi_x}{\partial t^2} - \delta_n \overline{\Lambda_5} \frac{\partial^2 \Phi_y}{\partial t^2}, \\ & sa_{21}W + sa_{22}\Phi_x + sa_{23}\Phi_y + y_6(W + \mu h) + y_7W(W + 2\mu h) \\ & = \overline{\Lambda_3} \Phi_{x,tt} - \lambda_m \overline{\Lambda_5} \frac{\partial^2 W}{\partial t^2}, \\ & sa_{31}W + sa_{32}\Phi_x + sa_{33}\Phi_y + y_8(W + \mu h) + y_9W(W + 2\mu h) \\ & = \overline{\Lambda_3} \Phi_{y,tt} - \delta_n \overline{\Lambda_5} \frac{\partial^2 W}{\partial t^2}. \end{aligned} \quad (37)$$

in which the detail of coefficients $sa_{1i}(i = \overline{1,5}), sa_{jk}(j = \overline{2,3}, k = \overline{1,3}), y_m(m = \overline{1,9})$ may be found in Appendix B.

2.3.2. Nonlinear vibration of PSP under thermal loadings

A simply supported PSP with immovable edges under thermal loads are considered. The condition expressing the immovability on the edges $u = 0$ on $x = 0, a$ and $v = 0$ on $y = 0, b$ is fulfilled on the average sense as [22]

$$\int_0^b \int_0^a \frac{\partial u}{\partial x} dx dy = 0, \int_0^a \int_0^b \frac{\partial v}{\partial x} dy dx = 0. \quad (38)$$

From Eqs. (11) and (22), one can obtain the following expressions in which Eq. (21)

$$\begin{aligned} \frac{\partial u}{\partial x} &= \Lambda_{11} \frac{\partial^2 f}{\partial y^2} - \Lambda_{12} \frac{\partial^2 f}{\partial x^2} + \Lambda_{13} \frac{\partial \phi_x}{\partial x} + \Lambda_{14} \frac{\partial \phi_y}{\partial y} - c_1\Lambda_{15} \left(\frac{\partial^2 w}{\partial x^2} + \frac{\partial \phi_x}{\partial x} \right) \\ &- c_1\Lambda_{16} \left(\frac{\partial^2 w}{\partial y^2} + \frac{\partial \phi_y}{\partial y} \right) + \Lambda_{17}\Phi_1 + \Lambda_{18}\Phi_2 - \frac{1}{2} \left(\frac{\partial w}{\partial x} \right)^2 - \frac{\partial w \partial w^*}{\partial x}, \\ \frac{\partial v}{\partial y} &= \Lambda_{21} \frac{\partial^2 f}{\partial x^2} - \Lambda_{12} \frac{\partial^2 f}{\partial y^2} + \Lambda_{23} \frac{\partial \phi_x}{\partial x} + \Lambda_{24} \frac{\partial \phi_y}{\partial y} - c_1\Lambda_{25} \left(\frac{\partial^2 w}{\partial x^2} + \frac{\partial \phi_x}{\partial x} \right) \\ &- c_1\Lambda_{26} \left(\frac{\partial^2 w}{\partial y^2} + \frac{\partial \phi_y}{\partial y} \right) + \Lambda_{27}\Phi_1 + \Lambda_{28}\Phi_2 - \frac{1}{2} \left(\frac{\partial w}{\partial y} \right)^2 - \frac{\partial w \partial w^*}{\partial y}. \end{aligned} \quad (39)$$

For to have Eq. (40), Eqs. (32–34) are used together with Eq. (38), the obtained results into Eq. (38). We have

$$\begin{aligned} N_{y0} &= f_1 W + f_4(W + 2\mu h)W + f_2\Phi_x + f_3\Phi_y + f_5\Phi_1 + f_6\Phi_2, \\ N_{x0} &= g_1 W + g_4(W + 2\mu h)W + g_2\Phi_x + g_3\Phi_y + g_5\Phi_1 + g_6\Phi_2. \end{aligned} \quad (40)$$

in which parameters $f_i(i = \overline{1,6}), g_i(i = \overline{1,6})$ are noted in Appendix C.

Table 3. The properties of material, is selected for the matrix.

Material	E (GPa)	ρ (kg/m ³)	ν	α/K
PmPV	(3.51 – 0.0047T)	1150	0.3	$45(1 + 0.0005\Delta T) \times 10^{-6}$
PMMA	(3.52 – 0.00347T)	1150	0.34	$45(1 + 0.0005\Delta T) \times 10^{-6}$
Ti-6Al-4V	122.56(1 – 0.004568T)	4429	0.29	$7.5788(6.638 \times 10^{-4}T - 3.147 \times 10^{-6}T^2)$

$$\begin{aligned}
& sa_{11}W + sa_{12}\Phi_x + sa_{13}\Phi_y + sa_{14}(W + \mu h)\Phi_x \\
& + sa_{15}(W + \mu h)\Phi_y + y_1^1(W + \mu h) \\
& + y_2^1W(W + \mu h) + y_3W(W + 2\mu h) \\
& + y_4^1W(W + \mu h)(W + 2\mu h) \\
& + y_5q = \Lambda_0 \frac{\partial^2 W}{\partial t^2} + 2\varepsilon\Lambda_1 \frac{\partial W}{\partial t} - \lambda_m \overline{\overline{\Lambda_5}} \frac{\partial^2 \Phi_x}{\partial t^2} - \delta_n \overline{\overline{\Lambda_5^*}} \frac{\partial^2 \Phi_y}{\partial t^2}, \\
& sa_{21}W + sa_{22}\Phi_x + sa_{23}\Phi_y + y_6(W + \mu h) \\
& + y_7W(W + 2\mu h) = \overline{\overline{\Lambda_3}} \frac{\partial^2 \Phi_x}{\partial t^2} - \lambda_m \overline{\overline{\Lambda_5}} \frac{\partial^2 W}{\partial t^2}, \\
& sa_{31}W + sa_{32}\Phi_x + sa_{33}\Phi_y + y_8(W + \mu h) + y_9W(W + 2\mu h) \\
& = \overline{\overline{\Lambda_3^*}} \frac{\partial^2 \Phi_y}{\partial t^2} - \delta_n \overline{\overline{\Lambda_5^*}} \frac{\partial^2 W}{\partial t^2}.
\end{aligned} \tag{41}$$

In order to obtain Eq. (41), Eq. (40) is replaced into Eqs. (37) and in which $sa_{14}^1, sa_{15}^1, y_1^1, y_2^1, y_4^1$ are noted in Appendix C.

Equation (41) is the basic equation governing of the non-linear vibration for imperfect PSP supported by elastic foundations in thermal environment. To solve this equation, the fourth-order Runge–Kutta method is used.

2.3.3. Natural frequency

In the case of $q = 0$, the natural frequencies of the perfect can be determined by solving the following equation

$$\begin{vmatrix}
sa_{11} + y_1^1 + \Lambda_0\omega^2 & sa_{12} - \lambda_m \overline{\overline{\Lambda_5}}\omega^2 & sa_{13} - \delta_n \overline{\overline{\Lambda_5^*}}\omega^2 \\
sa_{21} + y_6 - \lambda_m \overline{\overline{\Lambda_5}}\omega^2 & sa_{22} + \overline{\overline{\Lambda_3}}\omega^2 & sa_{23} \\
sa_{31} + y_8 - \delta_n \overline{\overline{\Lambda_5^*}}\omega^2 & sa_{32} & sa_{33} + \overline{\overline{\Lambda_3^*}}\omega^2
\end{vmatrix} = 0. \tag{42}$$

3. Results and discussion

After establishing Eqs. (41–42) for the dynamic response and natural frequency of the PSP with the influence of geometrical parameters, imperfection, elastic foundations, the volume fraction of CNTs and type of porosity distribution. The numerical results will be presented in this section. For the face sheets, the nano carbon tubes are arranged in the matrix, are made of poly (methyl methacrylate), mentioned as PMMA; PmPV or Ti-6Al-4V. Based on [40], the material properties of the three materials are shown in Table 3.

3.1. Validation of modeling

In order to increase the authenticity of this study, cross-checking the results is considered as one of the important parts. Table 4 shows the numerical results of this paper are compared to the results of Wang [36] and Natarajan et al.

[35] based on the higher-order structural theory with variables value as core to face sheet thickness h_c/h_f and CNTs volume fraction V_{CNT} . It can be observed from Table 3 that the discrepancy in the dimensionless frequencies in three cases is not significant. In the case of comparison with Wang and Shen [36], the largest difference is about 0.0808% with $h_c/h_f = 4$ and $V_{CNT} = 0.17$. In the case of comparison with Natarajan et al. [35], the largest difference is about 0.1105% with $h_c/h_f = 4$ and $V_{CNT} = 0.28$. Besides, Table 4 has remarkable value with $h_c/h_f = 6$ and $V_{CNT} = 0.17$, the dimensionless frequencies are not changed.

Next, with the effect of CNTs volume fraction, mode (m, n) and distribution of CNTs, the comparison of the non-dimensional frequencies with Shen and Wang [8] based on a higher-order shear deformation plate theory and Zhu et al. [7] based on the first-order shear deformation plate theory are tabulated in Table 5. Generally, the nondimensionless frequencies are not too different, it can explain due to used methods. Furthermore, the nondimensionless frequencies will increase when the CNTs volume fraction, mode (m, n) raise. Among two types: FG-O and FG-X, the nondimensionless frequencies with FG-X give a higher value than the non-dimensional frequencies with FG-O.

According to the above comments and Tables 4 and 5; we can see that the results of this paper are quite similar to the existing results. Therefore, it demonstrates that the approach, present method and the obtained results in this research are reliable and accurate.

3.2. Natural frequency

The influence of distribution of CNTs, width to total thickness ratio b/h and temperature changes on the natural frequencies are presented in Table 6. The natural frequencies of PSP will decrease when the temperature or ratio b/h raise. In addition, FG-V will have the highest natural frequency in three cases: FG-OO, FG-AV and FG-XX. In contrast, the lowest natural frequency will be the case FG-OO.

The natural frequencies of PSP with the effect of porosity distribution, length to weight ratio a/b and core to face sheet thickness h_c/h_f are recognized in Table 6. It can be seen that the ratio a/b raises results in natural frequencies of PSP decrease. It is interesting that the type porosity distribution has the positive effect on the modelings. Specifically, the porosity distribution is nonuniform symmetric will give the natural frequencies value higher than the remaining two porosity distribution types. Uniform distribution will obtain the lowest natural frequencies in three cases: Uniform distribution, nonuniform symmetric porosity distribution, nonuniform asymmetric porosity distribution.

Table 7 shows the influence of CNTs volume fraction V_{CNT} , the coefficient of porosity e_0 and elastic foundations on the natural frequencies of PSP. The natural frequencies of modelings will raise when CNTs volume fraction V_{CNT} ,

Table 4. Comparison of the dimensionless frequencies $\tilde{\Omega} = \Omega(a^2/h)\sqrt{\rho_c/E_c}$ for sandwich plates with CNTRC face sheets in thermal environments ($a/b = 1, b/h = 20$).

h_c/h_f	Source	$V_{CNT} = 0.12$	$V_{CNT} = 0.17$	$V_{CNT} = 0.28$
4	Wang and Shen [36]	4.6845	5.0763	5.7131
	Natarajan et al. [35]	4.6808	5.0697	5.7025
	Present	4.6819	5.0722	5.7088
6	Wang and Shen [36]	4.9119	5.1905	5.6569
	Natarajan et al. [35]	4.9111	5.1881	5.6524
	Present	4.9103	5.1881	5.6544
8	Wang and Shen [35]	5.0775	5.2927	5.6588
	Present	5.0764	5.2909	5.6571

Table 5. Comparison of the nondimensionless frequencies $\tilde{\omega} = \Omega(a^2/h)\sqrt{\rho_0/E_0}$ of CNTRC plates ($a/b = 1, b/h = 50, T = 300K$).

V_{CN}^*	Mode	Source	Shen and Wang [8]	Zhu et al. [7]	Present
0.11	(1, 1)	FG-O	14.138	14.302	14.264
		FG-X	23.143	22.984	23.024
	(1, 2)	FG-O	18.950	19.373	19.249
0.14	(1, 1)	FG-X	27.263	26.784	26.718
		FG-O	15.667	15.801	15.796
	(1, 2)	FG-X	25.831	25.555	25.670
0.17	(1, 1)	FG-O	20.184	20.563	20.478
		FG-X	29.879	29.192	29.196
	(1, 2)	FG-O	17.351	17.544	17.506
	(1, 1)	FG-X	28.625	28.413	28.421
		FG-O	23.283	23.783	23.659
	(1, 2)	FG-X	34.034	33.434	33.293

the coefficient of porosity e_0 or elastic foundations increase. Elastic foundations are one remarkable point in Table 8 because elastic foundations have a significant influence on the natural frequencies of PSP than CNTs volume fraction V_{CNT} , the coefficient of porosity e_0 . Especially, the natural frequencies of modelings will raise about three times when PSP is associated with Winkler foundation and Pasternak foundations.

The influence of matrix material and mode (m, n) on the natural frequencies of PSP are depicted in Table 9. It is clear that Ti-6Al-4V has the largest elastic modulus (Table 3) because the matrix material Ti-6Al-4V will give the highest natural frequencies value. Moreover, the face sheet FG-AV has effect beneficial than FG-XX and FG-OO on the natural frequencies. In contrast, in three types of face sheets, FG-OO has the worst influence. The natural frequencies of PSP also raise when mode (m, n) increases.

3.3. Dynamic responses

3.3.1. The effect of volume fraction CNTs, porous distribution and material of matrix

A study on the influence of matrix materials are carried out and remarkable results are shown in Figure 5. Three matrix materials are considered as PMMA; PmPV or Ti-6Al-4V. It can be seen that Ti-6Al-4V denotes positive influence on the amplitude deflection-time curve of PSP because elastic modulus of Ti-6Al-4V is the biggest. In this case, $T=0$, modulus of Ti-6Al-4V is 122.56 GPA much bigger modulus of PmPV and PMMA are 3.51 and 3.52 GPA, respectively.

Table 6. The natural frequencies of PSP with the effect of type distribution of CNTs, weight to total thickness ratio b/h and thermal loadings.

ΔT	Face sheet	$b/h = 10$	$b/h = 15$	$b/h = 20$
0	FG-OO	12091.6	8182.9	6170.3
	FG-AV	12168.3	8234.9	6209.7
	FG-XX	12096.2	8185.8	6172.5
50	FG-OO	11445.4	7322.1	5040.1
	FG-AV	11525.7	7379.7	5087.8
	FG-XX	11450.3	7325.4	5042.8
100	FG-OO	10709.7	6256.1	3404.5
	FG-AV	10795.0	6323.1	3474.2
	FG-XX	10714.8	6257.0	3408.4

Table 7. The influence of CNTs volume fraction V_{CNT} , the coefficient of porosity e_0 and elastic foundations on the natural frequencies of PSP.

e_0	(k_1, k_2)	$V_{CNT} = 0.12$	$V_{CNT} = 0.17$	$V_{CNT} = 0.28$
0	(0, 0)	6199.7	6461.9	6909.1
	(0.1, 0)	6409.0	6662.7	7097.0
	(0.1, 0.02)	17362.0	17452.3	17612.0
0.2	(0, 0)	6209.7	6487.9	6960.9
	(0.1, 0)	6432.3	6701.2	7159.8
	(0.1, 0.02)	17866.8	17959.9	18124.1
0.4	(0, 0)	6250.5	6548.3	7052.3
	(0.1, 0)	6489.7	6776.8	7264.6
	(0.1, 0.02)	18517.2	18613.6	18783.3

In order to consider the effect of CNT on the amplitude deflection-time curve of PSP, we consider the effect of CNT volume fractions with value as 0.12, 0.17 and 0.28 in Figure 6. Under the same conditions, increasing of CNT volume fractions results in the amplitude deflection decreases. It demonstrates that the volume fractions of CNT have an important contribution in reducing the vibration of PSP.

The vibration of PSP with the effect of coefficient of porosity is shown in Figure 7. It indicates that when the coefficient of porosity increases results in the amplitude of vibration increases. It demonstrates that materials with many porous will not adversely affect the amount of material.

The effect of porous distribution like uniform distribution, nonuniform distribution 1 (symmetric) and nonuniform distribution 2 (asymmetric) on the vibration of PSP are recognized in Figure 8. The Figure 8 indicates that the nondistribution has a positive influence and in nonuniform distribution, the symmetric has a higher influence with deflection reduces about 3.57% (it compared to the influence of uniform distribution) while the effect of Asymmetric is negligible. It can be seen that the amplitude deflection with the influence of uniform distribution and asymmetric is almost similar. Therefore, in the figures, this paper chose the symmetric (nonuniform distribution 1) to the investigate dynamic behavior of PSP with another factor.

3.3.2. The influence of geometrical parameter, viscous damping and elastic foundations

In order to investigate the geometrical parameter of PSP on the dynamic response. Figures 9 and 10 show the influence

Table 8. The natural frequencies of PSP with the effect of porosity distribution, length to width ratio a/b and core to face sheet thickness of h_c/h_f .

h_c/h_f	a/b	Nonuniform symmetric porosity	Nonuniform asymmetric porosity	Uniform porosity
4	1	5757.1	5667.6	5652.3
	1.5	3683.0	3608.8	3595.7
	2	3029.2	2961.1	2949.1
6	1	6017.4	5904.2	5884.4
	1.5	4021.4	3931.7	3915.8
	2	3375.6	3295.1	3280.8
8	1	6209.6	6082.1	6059.7
	1.5	4240.8	4141.9	4124.5
	2	3592.6	3504.7	3489.2

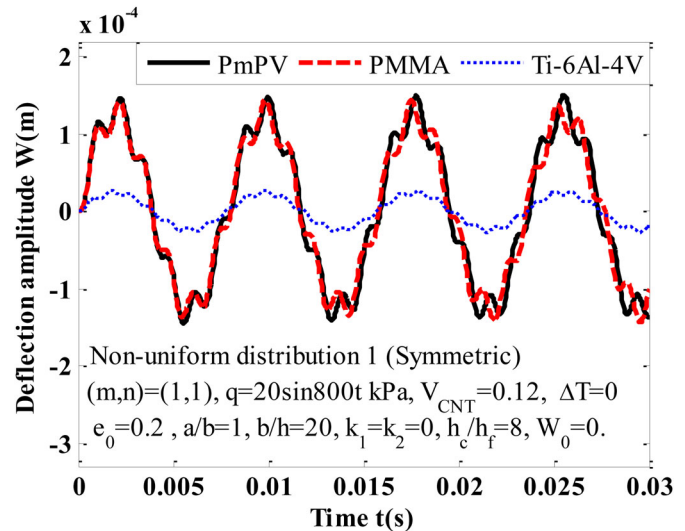
Table 9. The influence of matrix material and mode (m, n) on the natural frequencies of PSP.

(m, n)	Face sheet	PmPV	PMMA	Ti-6Al-4V
(1, 1)	FG-OO	4711.1	4789.4	6170.4
	FG-AV	4852.2	4932.8	6209.6
	FG-XX	4722.1	4800.0	6172.5
(1, 2)	FG-OO	6634.9	6860.5	14183.4
	FG-AV	6740.8	6946.7	14201.4
	FG-XX	6643.3	6868.5	14184.4
(2, 1)	FG-OO	15168.3	15580.5	17101.2
	FG-AV	15651.0	16149.0	17319.7
	FG-XX	15230.2	15640.2	17114.1
(2, 2)	FG-OO	16137.0	16641.4	24183.1
	FG-AV	16584.4	17160.4	24336.6
	FG-XX	16195.4	16697.5	24192.4

of the core to face sheet thickness ratio and imperfection parameter, respectively. As can be seen, the amplitude of deflection increases when increasing of h_c/h_f ratio from Figure 9. It can be explained that reducing of the stiffness of core is a consequence of the h_c/h_f ratio increases. In addition, Figure 10 indicates that the initial imperfection parameter ascends leads to increase the vibration of PSP.

Figures 11 and 12 depict vibration of PSP with the influence of the width to total thickness ratio b/h and the length to width ratio a/b , respectively. The dynamic behavior of PSP increases when the ratio b/h and a/b increase. Specifically, PSP with conditions $V_{CNT} = 0.12$, $e_0 = 0.2$, $\Delta T = 0$, $a/b = 1$, $k_1 = k_2 = 0$, $h_c/h_f = 8$, $W_0 = 0$ and review time $t = [0, 0.03](s)$, the width to total thickness ratio b/h increases two times (from 10 to 20) results in amplitude of deflection increases approximately 14 times while the length to width ratio a/b increases from 1 to 2 leads to vibration of PSP raise about 300% (three times). It demonstrates that the influence of ratio b/h bigger than the influence of ratio a/b .

In this research, PSP is associated with elastic foundations and the effect of elastic foundations: Winkler foundation and Pasternak foundation on the amplitude deflection–time is depicted in Figures 13 and 14, respectively. In these figures, this paper considers elastic foundations (k_1, k_2) with mode value. It can be seen that the elastic foundations have positive effect on the PSP. In other words, the dynamic behavior of PSP is enhanced by elastic foundations. In addition, the effect of Winkler foundation is lower than the influence of Pasternak foundation. The Winkler change from 0 to 0.3 GPa/m leads to reduce amplitude deflection

**Figure 5.** The effect of matrix materials on the amplitude deflection–time curve of PSP.

about 27.3% while the Pasternak change from 0 to 0.03 GPa/m leads to reduce amplitude deflection about 25 times. This can be explained by the relationship between Pasternak foundation and deflection are nonlinear. In contrast, the relationship between Winkler foundation and deflection is linear.

The vibration of PSP with the viscous damping is shown in Figure 15. It indicates that the viscous damping increase results in the amplitude of vibration decreases but the change was not great.

3.3.3. The influence of mechanical loadings and thermal loadings

Besides imperfection, geometrical parameters, elastic foundations, porosity distribution, CNT volume fraction, the influence of mechanical loads on the vibration of PSP is shown in Figure 16. The amplitude deflection ascends when the mechanical loads are intensified. Figure 17 shows the influence of thermal loads on the vibration of PSP with $V_{CNT} = 0.12$, $e_0 = 0.2$, $\Delta T = 0$, $a/b = 1$, $b/h = 20$, $k_1 = k_2 = 0$, $h_c/h_f = 8$, $W_0 = 0$. It can be seen that the thermal loads have a negative influence on the deflection of PSP. Increasing the temperature makes deflection raises significantly from 2.5 to 10.2 mm (about 3.08 times).

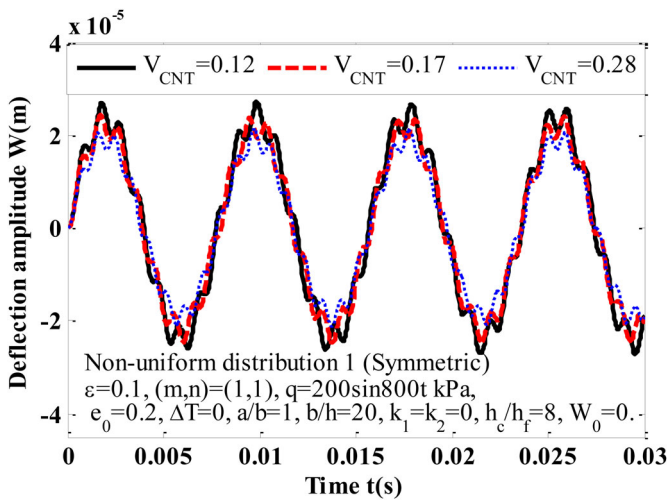


Figure 6. The influence of CNT volume fraction on the amplitude deflection–time curve of PSP.

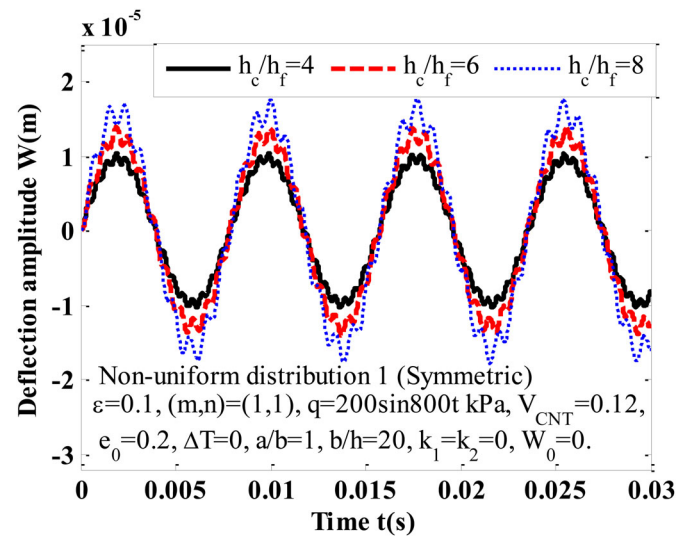


Figure 9. The influence of core to face sheet thickness ratio on the vibration of PSP.

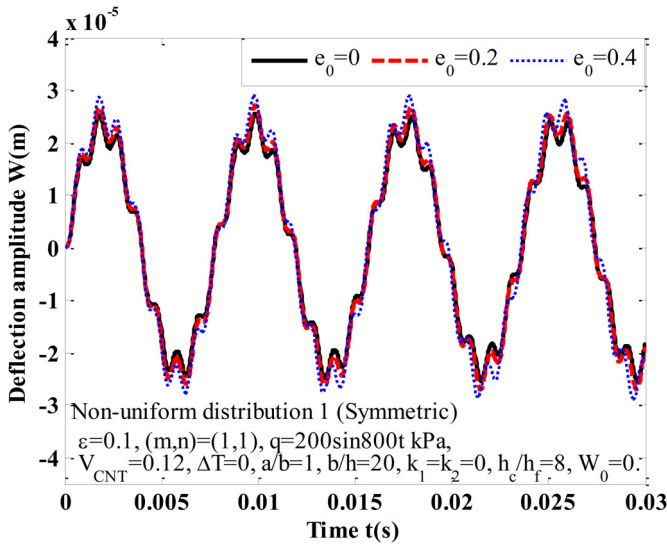


Figure 7. Vibration of PSP with change of coefficient of porosity.

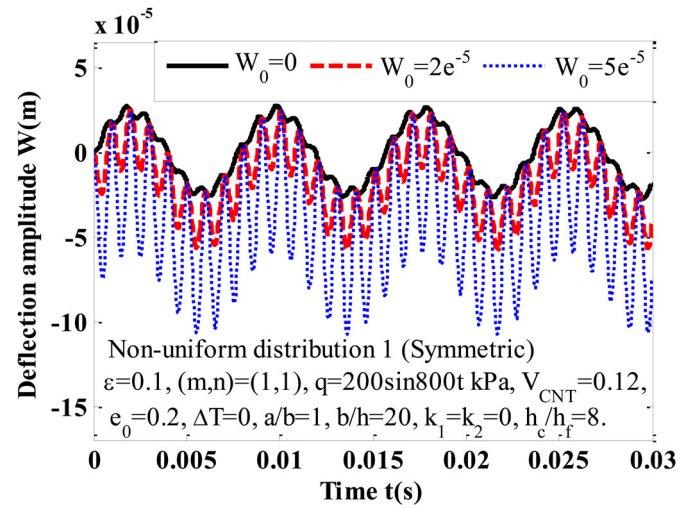


Figure 10. Amplitude of deflection–time with effect of initial imperfection parameter.

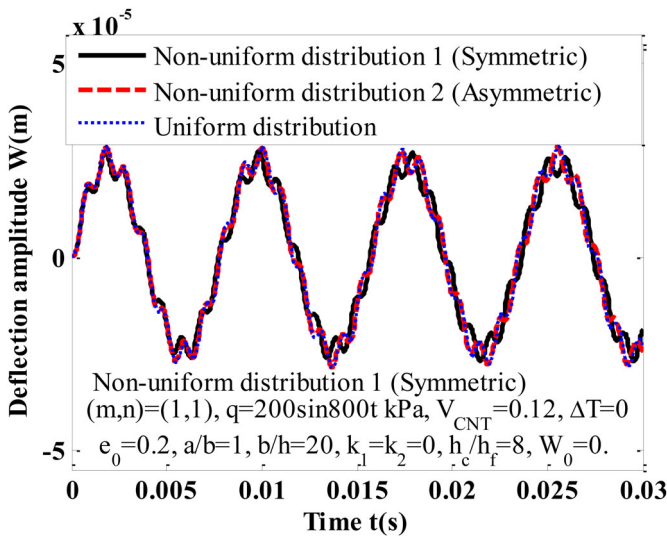


Figure 8. Vibration of PSP with change of porous distribution.

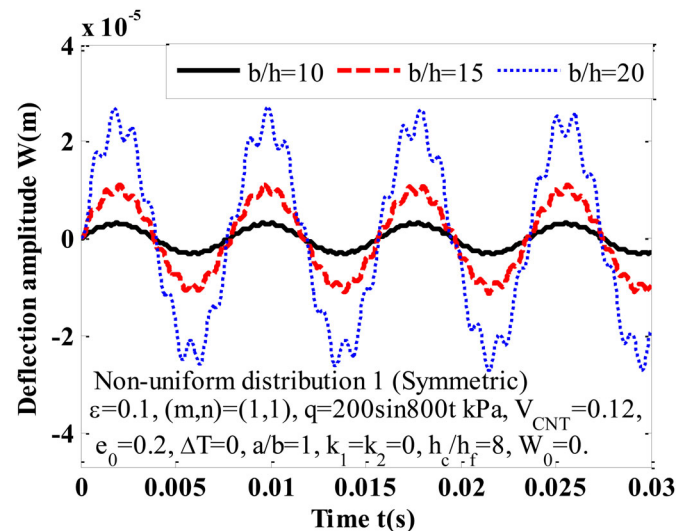


Figure 11. Dynamic behavior of PSP with the influence of ratio b/h .

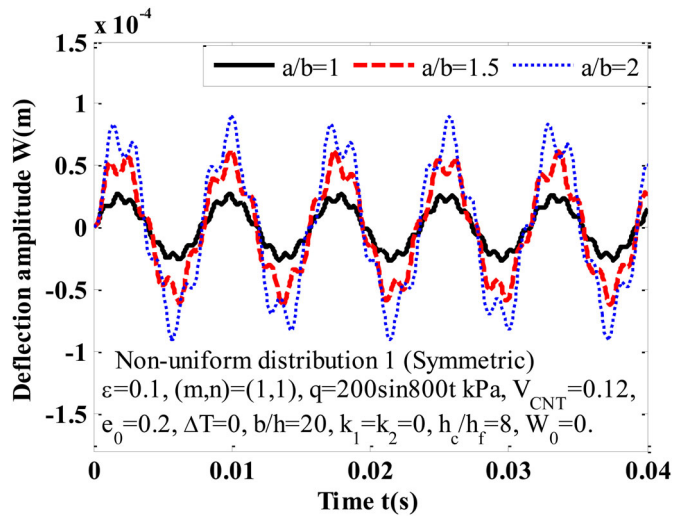


Figure 12. Dynamic behavior of PSP with the influence of ratio a/b .

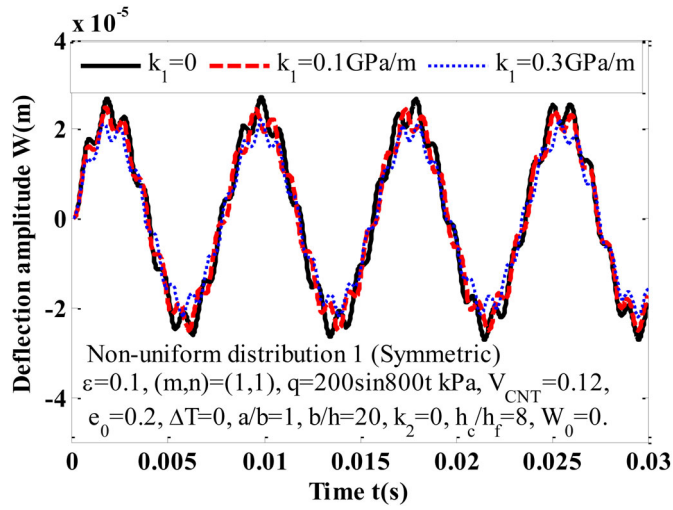


Figure 13. The influence of Winkler foundation on the dynamic response of PSP.

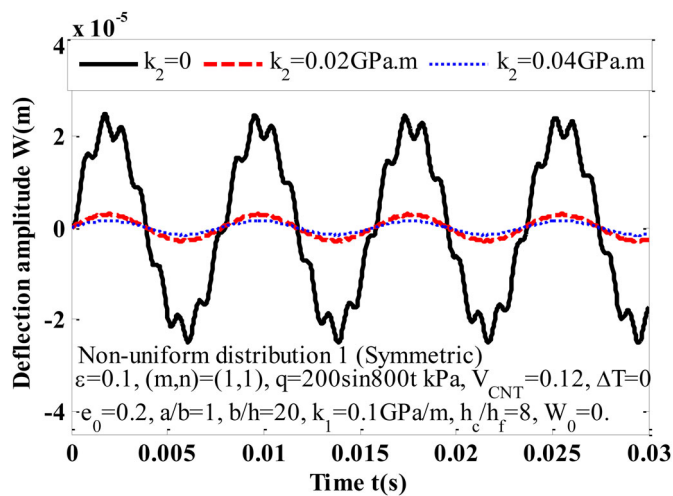


Figure 14. The influence of Pasternak foundation on the dynamic response of PSP.

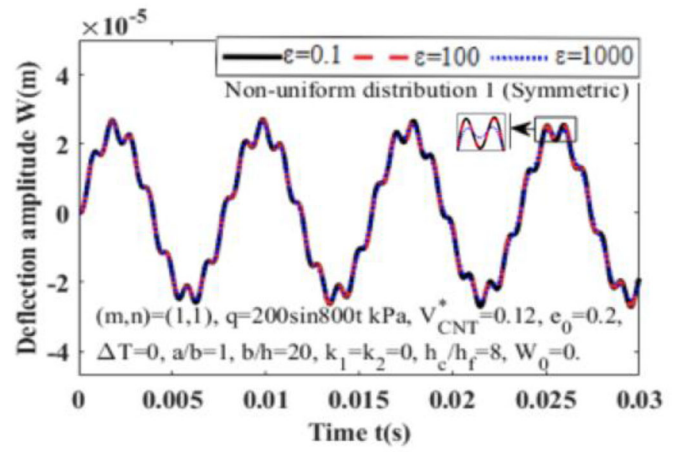


Figure 15. Vibration of PSP with the effect of the viscous damping.

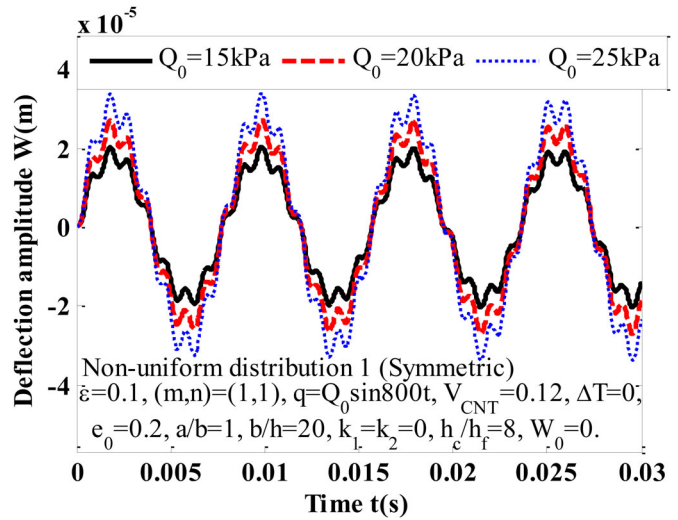


Figure 16. Vibration of PSP with the effect of mechanical loads.

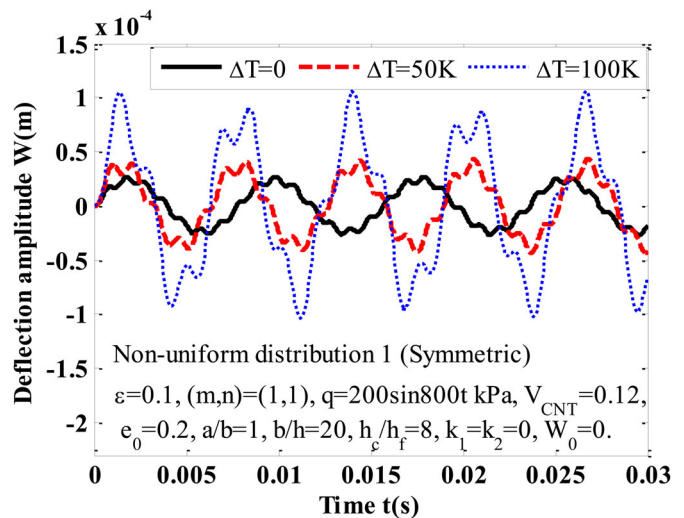


Figure 17. Vibration of PSP with the effect of thermal loads.

4. Conclusions

Because of the outstanding properties of advanced materials, the advanced materials are widely used in aerospace engineering so mechanical load capacity and temperature resistance of materials play an important role. In this paper, the influence of CNTs, porosity, geometrical parameters, mechanical and thermal loads on the vibration and dynamic response of the FG-CNTRC sandwich plate is investigated.

The plate is made by three layers in which the core layer is porous FGM materials, bottom and top surfaces are FG-CNTRC and the sandwich plate is resting on elastic foundations. Based on Hamilton's principle and analytical solutions the motion equation is given. In order to determine the results of dynamic analysis, the Reddy's TSDT and Galerkin method are used. Furthermore, the natural frequencies of structural are obtained by using the fourth-order Runge–Kutta method. The remarkable points can observe as:

- The present approach, methodology and obtained results are verified as reliable and accurate by comparing the obtained results with the existing results.
- In nonuniform distribution, the symmetric has a higher influence with deflection reduces about 3.57% (it compared to the influence of uniform distribution) while the effect of asymmetric is negligible.
- Ti–6Al–4V denotes a positive influence on the amplitude deflection–time curve of PSP because the elastic modulus of Ti–6Al–4V is the biggest.
- The volume fractions of CNT have an important contribution in reducing the vibration of PSP. The volume fractions of CNT increase results in deflection of PSP decrease.
- The amplitude of deflection increases when increasing of h_c/h_f ratio and initial imperfection parameter ascends leads to increase vibration of PSP.
- The width to total thickness ratio b/h increases two times (from 10 to 20) results in amplitude of deflection increase approximately 14 times while the length to width ratio a/b increases from 1 to 2 leads to vibration of PSP raise about 300% (three times).
- The Winkler parameters change from 0 to 0.3 GPa/m leads to reduce amplitude deflection about 27.3% while the Pasternak parameters change from 0 to 0.03 GPa m leads to reduce amplitude deflection about 25 times.
- When increasing the viscous damping results in the amplitude of vibration decreases.
- The amplitude deflection ascends when the mechanical loads are intensified.
- Increasing temperature makes deflection raised significantly from 2.5 to 10.2 mm (about 3.08 times).

Disclosure statement

The authors declare no conflict of interest.

Funding

This research is funded by Vietnam National Foundation for Science and Technology Development (NAFOSTED) under grant number 107.02-2018.04. The authors are grateful for this support.

References

- [1] X.W. Chen, and Z.Q. Yue, Contact mechanics of two elastic spheres reinforced by functionally graded materials (FGM) thin coatings, *Eng. Anal. Bound. Elem.*, vol. 109, pp. 57–69, 2019.
- [2] A.H. Sofiyev, The buckling and vibration analysis of coating-FGM-substrate conical shells under hydrostatic pressure with mixed boundary conditions, *Compos. Struct.*, vol. 209, pp. 686–693, 2019.
- [3] R. Kolahchi, M. Safari, and M. Esmailpour, Dynamic stability analysis of temperature-dependent functionally graded CNT-reinforced visco-plates resting on orthotropic elastomeric medium, *Compos. Struct.*, vol. 150, pp. 255–265, 2016.
- [4] N.D. Duc, Nonlinear dynamic response of imperfect eccentrically stiffened FGM double curved shallow shells on elastic foundation, *J. Compos. Struct.*, vol. 102, pp. 306–314, 2013.
- [5] H. Lin, D. Cao, C. Shao, and Y. Xu, Studies for aeroelastic characteristics and nonlinear response of FG-CNT reinforced composite panel considering the transient heat conduction, *Compos. Struct.*, vol. 188, pp. 470–482, 2018.
- [6] S.H. Shen, Thermal buckling and postbuckling behavior of functionally graded carbon nanotube-reinforced composite cylindrical shells, *Compos. Part B*, vol. 43, no. 3, pp. 1030–1038, 2012.
- [7] P. Zhu, Z.X. Lei, and K.M. Liew, Static and free vibration analyses of carbon nanotube reinforced composite plates using finite element method with first order shear deformation plate theory, *Compos. Struct.*, vol. 94, no. 4, pp. 1450–1460, 2012.
- [8] H.S. Shen, and H. Wang, Nonlinear vibration of compressed and thermally postbuckled nanotube-reinforced composite plates resting on elastic foundations, *Aerosp. Sci. Technol.*, vol. 64, pp. 63–74, 2017.
- [9] S.H. Shen and Y. Xiang, Nonlinear bending of nanotube-reinforced composite cylindrical panels resting on elastic foundations in thermal environments, *Eng. Struct.*, vol. 80, pp. 163–172, 2014.
- [10] V. Bhagat, P. Jeyaraj, and S.M. Murigendrappa, Buckling and free vibration behavior of a temperature dependent FG-CNTRC cylindrical panel under thermal load, *Mater. Today 2018: Proc.*, vol. 5, no. 11, pp. 23682–23691, 2018.
- [11] S.H. Shen, Postbuckling of nanotube-reinforced composite cylindrical shells in thermal environments. Part II: pressure-loaded shells, *Compos. Struct.*, vol. 93, no. 10, pp. 2496–2503, 2011.
- [12] Y. Kiani, Analysis of FG-CNT reinforced composite conical panel subjected to moving load using Ritz method, *Thin-Walled Struct.*, vol. 119, pp. 47–57, 2017.
- [13] Y. Kiani, Thermal buckling of temperature-dependent FG-CNT-reinforced composite skew plates, *J. Therm. Stresses.*, vol. 40, no. 11, pp. 1442–1460, 2017.
- [14] Yaser Kiani, Rossana Dimitri, and Francesco Tornabene, Free vibration study of composite conical panels reinforced with FG-CNTs, *Eng. Struct.*, vol. 172, pp. 472–482, 2018.
- [15] Y. Kiani, Free vibration of carbon nanotube reinforced composite plate on point supports using Lagrangian multipliers, *Meccanica*, vol. 52, no. 6, pp. 1353–1367, 2017.
- [16] Y. Kiani, Dynamics of FG-CNT reinforced composite cylindrical panel subjected to moving load, *Thin-Walled Struct.*, vol. 111, pp. 48–57, 2017.
- [17] Y. Kiani, Free vibration of FG-CNT reinforced composite spherical shell panels using Gram-Schmidt shape functions, *Compos. Struct.*, vol. 159, pp. 368–381, 2017.

- [18] Z.X. Lei, L.W. Zhang, and K.M. Liew, Vibration of FG-CNT reinforced composite thick quadrilateral plates resting on Pasternak foundations, *Eng. Anal. Bound. Elem.*, vol. 64, pp. 1–11, 2016.
- [19] L.W. Zhang, Z.G. Song, and K.M. Liew, State-space Levy method for vibration analysis of FG-CNT composite plates subjected to in-plane loads based on higher-order shear deformation theory, *Compos. Struct.*, vol. 134, pp. 989–1003, 2015.
- [20] B. Qin, R. Zhong, T. Wang, Q. Wang, Y. Xu, and Z. Hu, A unified Fourier series solution for vibration analysis of FG-CNTRC cylindrical, conical shells and annular plates with arbitrary boundary conditions, *Compos. Struct.*, vol. 232, pp. 111549, 2020.
- [21] P. Jiao, Z. Chen, Y. Li, H. Ma, and J. Wu, Dynamic buckling analyses of functionally graded carbon nanotubes reinforced composite (FG-CNTRC) cylindrical shell under axial power-law time-varying displacement load, *Compos. Struct.*, vol. 220, pp. 784–797, 2019.
- [22] N.D. Khoa, Anh Vm, and N.D. Duc, Nonlinear dynamic response and vibration of functionally graded nanocomposite cylindrical panel reinforced by carbon nanotubes in thermal environment, *J. Sandwich Struct. Mater.*, 2016. DOI: [10.1177/1099636219847191](https://doi.org/10.1177/1099636219847191).
- [23] K. Foroutan, A. Shaterzadeh, and H. Ahmadi, Nonlinear static and dynamic hygrothermal buckling analysis of imperfect functionally graded porous cylindrical shells, *Appl. Math. Modell.*, vol. 77, no. 1, pp. 539–553, 2020. DOI: [10.1016/j.apm.2019.07.062](https://doi.org/10.1016/j.apm.2019.07.062).
- [24] C.Z. Qin, B. Guo, M. Celia, and R. Wu, Dynamic pore-network modeling of air-water flow through thin porous layers, *Chem. Eng. Sci.*, vol. 202, pp. 194–207, 2019.
- [25] M.H. Jalaei and H.T. Thai, Dynamic stability of viscoelastic porous FG nanoplate under longitudinal magnetic field via a nonlocal strain gradient quasi-3D theory, *Compos. Part B: Eng.*, vol. 175, pp. 107164, 2019.
- [26] H.N. Li, P.F. Liu, C. Li, G. Li, and H. Zhan, Experimental research on dynamic mechanical properties of metal tailings porous concrete, *Constr. Build. Mater.*, vol. 213, pp. 20–31, 2019.
- [27] Di Wu, Airong Liu, Youqin Huang, Yonghui Huang, Yonglin Pi, and Wei Gao, Dynamic analysis of functionally graded porous structures through finite element analysis, *Eng. Struct.*, vol. 165, pp. 287–301, 2018.
- [28] M.H. Jalaei and Ö. Civalek, Ö. On dynamic instability of magnetically embedded viscoelastic porous FG nanobeam, *Int. J. Eng. Sci.*, vol. 143, pp. 14–32, 2019.
- [29] D. Chen, S. Kitiporncha, and J. Yang, Dynamic response and energy absorption of functionally graded porous structures, *Mater. Des.*, vol. 140, pp. 473–487, 2018.
- [30] P.H. Cong, T.M. Chien, N.D. Khoa, and N.D. Duc, Nonlinear thermomechanical buckling and post-buckling response of porous FGM plates using Reddy's HSDT, *Aerosp. Sci. Technol.*, vol. 77, pp. 419–428, 2018.
- [31] N. Ziane, S.A. Meftah, G. Ruta, and A. Tounsi, Thermal effects on the instabilities of porous FGM box beams, *Eng. Struct.*, vol. 134, pp. 150–158, 2017.
- [32] P.A. Demirhan and V. Taskin, Bending and free vibration analysis of Levy-type porous functionally graded plate using state space approach, *Compos. Part B: Eng.*, vol. 160, pp. 661–676, 2019.
- [33] B. Safaei, R.M. Dastjerdi, K. Behdinin, Z. Qin, and F. Chu, Thermoelastic behavior of sandwich plates with porous polymeric core and CNT clusters/polymer nanocomposite layers, *Compos. Struct.*, vol. 226, pp. 111209, 2019.
- [34] M.H. Hajmohammad, R. Kolahchi, M.S. Zarei, and A.H. Nouri, Dynamic response of auxetic honeycomb plates integrated with agglomerated CNT-reinforced face sheets subjected to blast load based on visco-sinusoidal theory, *Int. J. Mech. Sci.*, vol. 153–154, pp. 391–401, 2019.
- [35] S. Natarajan, M. Haboussi, and G. Manickam, The application of higher-order structural theory to bending and free vibration analysis of sandwich plates with CNT reinforced composite face sheets, *Compos. Struct.*, vol. 113, pp. 197–207, 2014.
- [36] Z.X. Wang, and H.S. hen, Nonlinear vibration and bending of sandwich plates with nanotube-reinforced composite face sheets, *Compos.: Part B.*, vol. 43, no. 2, pp. 411–421, 2012.
- [37] A.R. Saidi, R. Bahaadini, and K.M. Mozafari, On vibration and stability analysis of porous plates reinforced by graphene platelets under aerodynamical loading, *Compos. Part B.*, vol. 164, pp. 778–799, 2019.
- [38] Q. Li, D. Wu, X. Chen, L. Liu, Y. Yu, and W. Gao, Nonlinear vibration and dynamic buckling analyses of sandwich functionally graded porous plate with graphene platelet reinforcement resting on Winkler – Pasternak elastic foundation, *Int. J. Mech. Sci.*, vol. 148, pp. 596–610, 2018.
- [39] K. Mehar, S.K. Panda, Y. Devarajan, and G. Choubey, Numerical buckling analysis of graded CNT- reinforced composite sandwich shell structure under thermal loading, *Compos. Struct.*, vol. 216, pp. 406–414, 2019.
- [40] A. Sankar, S. Natarajan, and M. Ganapathi, Dynamic instability analysis of sandwich plates with CNT reinforced facesheets, *Compos. Struct.*, vol. 146, pp. 187–200, 2016.

Appendix A

$$SA_{11}(w) = TB_{11} \frac{\partial^2 w}{\partial x^2} + TB_{12} \frac{\partial^2 w}{\partial y^2} + TB_{13} \frac{\partial^4 w}{\partial x^4} + TB_{14} \frac{\partial^4 w}{\partial x^2 \partial y^2} + TB_{15} \frac{\partial^4 w}{\partial y^4} - k_1 w + k_2 \left(\frac{\partial^2 w}{\partial x^2} + \frac{\partial^2 w}{\partial y^2} \right),$$

$$SA_{12}(\phi_x) = TB_{11} \frac{\partial \phi_x}{\partial x} + TB_{16} \frac{\partial^3 \phi_x}{\partial x^3} + TB_{17} \frac{\partial^3 \phi_x}{\partial x \partial y^2},$$

$$SA_{13}(\phi_y) = TB_{12} \frac{\partial \phi_y}{\partial y} + TB_{18} \frac{\partial^3 \phi_y}{\partial y^3} + TB_{19} \frac{\partial^3 \phi_y}{\partial x^2 \partial y},$$

$$SA_{14}(\psi) = TB_{110} \frac{\partial^4 \psi}{\partial x^4} + TB_{111} \frac{\partial^4 \psi}{\partial x^2 \partial y^2} + TB_{112} \frac{\partial^4 \psi}{\partial y^4},$$

$$SA(w, \psi) = \frac{\partial^2 \psi}{\partial y^2} \frac{\partial^2 w}{\partial x^2} - 2 \frac{\partial^2 \psi}{\partial x \partial y} \frac{\partial^2 w}{\partial y^2} + \frac{\partial^2 \psi}{\partial x^2} \frac{\partial^2 w}{\partial y^2},$$

$$SA_{21}(w) = TB_{21} \frac{\partial w}{\partial x} + TB_{22} \frac{\partial^3 w}{\partial x^3} + TB_{23} \frac{\partial^3 w}{\partial x \partial y^2},$$

$$SA_{22}(\phi_x) = TB_{21} \phi_x + TB_{24} \frac{\partial^2 \phi_x}{\partial x^2} + TB_{25} \frac{\partial^2 \phi_x}{\partial y^2},$$

$$SA_{23}(\phi_y) = TB_{26} \frac{\partial^2 \phi_y}{\partial x \partial y}, SA_{24}(\psi) = TB_{27} \frac{\partial^3 \psi}{\partial x^3} + TB_{28} \frac{\partial^3 \psi}{\partial x \partial y^2},$$

$$SA_{31}(w) = TB_{31} \frac{\partial w}{\partial y} + TB_{32} \frac{\partial^3 w}{\partial x^2 \partial y} + TB_{33} \frac{\partial^3 w}{\partial y^3}, SA_{32}(\phi_x) = TB_{34} \frac{\partial^2 \phi_x}{\partial x \partial y},$$

$$SA_{33}(\phi_y) = TB_{31} \phi_y + TB_{35} \frac{\partial^2 \phi_y}{\partial x^2} + TB_{36} \frac{\partial^2 \phi_y}{\partial y^2}, SA_{34}(\psi) = TB_{37} \frac{\partial^3 \psi}{\partial x^2 \partial y} + TB_{38} \frac{\partial^3 \psi}{\partial y^3}.$$

$$TB_{11} = T_{44} - 6c_1 K_{44} + 9c_1^2 Y_{44}, TB_{12} = T_{55} - 6c_1 K_{55} + 9c_1^2 Y_{55}, TB_{13} = -c_1^2 (L_{11} \Lambda_{15} + L_{12} \Lambda_{25} + O_{11}),$$

$$TB_{14} = -c_1^2 (4L_{66} \Lambda_{33} + 4O_{66} + L_{11} \Lambda_{16} + L_{12} \Lambda_{26} + 2O_{12} + L_{12} \Lambda_{15} + L_{22} \Lambda_{25}),$$

$$TB_{15} = -c_1^2 (L_{12} \Lambda_{16} + L_{22} \Lambda_{26} + O_{22}), TB_{16} = c_1 (L_{11} \Lambda_{13} - c_1 L_{11} \Lambda_{15} + Y_{11} - c_1 O_{11} + L_{12} \Lambda_{23} - c_1 L_{12} \Lambda_{25}),$$

$$TB_{17} = c_1 (2L_{66} \Lambda_{32} - 2c_1 L_{66} \Lambda_{33} + 2K_{66} - 2c_1 O_{66} + c_1 L_{12} \Lambda_{13} - c_1 L_{12} \Lambda_{15} + Y_{12} - c_1 O_{12} + L_{22} \Lambda_{23} - c_1 L_{22} \Lambda_{25}),$$

$$TB_{18} = c_1 (L_{12} \Lambda_{14} - c_1 L_{12} \Lambda_{16} + L_{22} \Lambda_{24} - c_1 L_{22} \Lambda_{26} + Y_{22} - c_1 O_{22}),$$

$$TB_{19} = c_1 (2L_{66} \Lambda_{32} - 2c_1 L_{66} \Lambda_{33} + 2Y_{66} - 2c_1 O_{66} + L_{11} \Lambda_{14} - c_1 L_{11} \Lambda_{16} + L_{12} \Lambda_{24} - c_1 L_{12} \Lambda_{26} + Y_{12} - c_1 O_{12}),$$

$$TB_{110} = -c_1 (L_{11} \Lambda_{12} - L_{12} \Lambda_{21}), TB_{112} = c_1 (L_{12} \Lambda_{11} - L_{22} \Lambda_{12}),$$

$$TB_{111} = -c_1 (2L_{66} \Lambda_{31} - L_{11} \Lambda_{11} + 2L_{12} \Lambda_{12} - L_{22} \Lambda_{21}),$$

$$TB_{21} = -T_{44} + 6c_1 K_{44} - 9c_1^2 F_{44}, TB_{22} = -c_1 (H_{11} \Lambda_{15} + Y_{11} + H_{12} \Lambda_{25} - c_1 L_{11} \Lambda_{15} - c_1 O_{11} - c_1 L_{12} \Lambda_{25}),$$

$$TB_{23} = -c_1 (H_{11} \Lambda_{16} + H_{12} \Lambda_{26} + Y_{12} + 2H_{66} \Lambda_{33} + 2Y_{66} - 2c_1 L_{66} \Lambda_{33} - 2c_1 O_{66} - c_1 L_{11} \Lambda_{16} - c_1 L_{12} \Lambda_{26} - c_1 O_{12}),$$

$$TB_{24} = H_{11} \Lambda_{13} - c_1 H_{11} \Lambda_{15} + K_{11} - c_1 Y_{11} + H_{12} \Lambda_{23} - c_1 H_{12} \Lambda_{25} - c_1 H_{11} \Lambda_{13} + c_1^2 L_{11} \Lambda_{15} - c_1 Y_{11} + c_1^2 O_{11}$$

$$- c_1 L_{12} \Lambda_{23} + c_1^2 L_{12} \Lambda_{25},$$

$$TB_{25} = H_{66} \Lambda_{32} - c_1 H_{66} \Lambda_{33} + K_{66} - c_1 Y_{66} - c_1 L_{66} \Lambda_{32} + c_1^2 L_{66} \Lambda_{33} - c_1 Y_{66} + c_1^2 O_{66},$$

$$TB_{26} = H_{11} \Lambda_{14} - c_1 H_{11} \Lambda_{16} + H_{12} \Lambda_{24} - c_1 H_{12} \Lambda_{26} + K_{12} - c_1 Y_{12} + H_{66} \Lambda_{32} - c_1 H_{66} \Lambda_{33} + K_{66} - c_1 Y_{66} - c_1 L_{66} \Lambda_{32}$$

$$+ c_1^2 L_{66} \Lambda_{33} - c_1 Y_{66} + c_1^2 O_{66} - c_1 L_{11} \Lambda_{14} + c_1^2 L_{11} \Lambda_{16} - c_1 L_{12} \Lambda_{24} + c_1^2 L_{12} \Lambda_{26} - c_1 Y_{12} + c_1^2 O_{12},$$

$$TB_{27} = -H_{11} \Lambda_{12} + H_{12} \Lambda_{21} + c_1 L_{11} \Lambda_{12} - c_1 L_{12} \Lambda_{21},$$

$$TB_{28} = H_{11} \Lambda_{11} - H_{12} \Lambda_{12} - H_{66} \Lambda_{31} - c_1 L_{11} \Lambda_{11} + c_1 L_{12} \Lambda_{12} + c_1 L_{66} \Lambda_{31},$$

$$TB_{31} = -T_{55} + 6c_1 K_{55} - 9c_1^2 Y_{55},$$

$$TB_{32} = -c_1 (2H_{66} \Lambda_{33} + 2Y_{66} + H_{12} \Lambda_{15} + Y_{12} + H_{22} \Lambda_{25} - 2c_1 L_{66} \Lambda_{33} - 2c_1 O_{66} - c_1 L_{12} \Lambda_{15} - c_1 O_{12} - c_1 L_{22} \Lambda_{25}),$$

$$TB_{33} = -c_1 (H_{12} \Lambda_{16} + H_{22} \Lambda_{26} + Y_{22} - c_1 L_{12} \Lambda_{16} - c_1 L_{22} \Lambda_{26} - c_1 O_{22}),$$

$$TB_{34} = H_{66} \Lambda_{32} - c_1 H_{66} \Lambda_{33} + K_{66} - c_1 Y_{66} + H_{12} \Lambda_{13} - c_1 H_{12} \Lambda_{15} + K_{12} - c_1 Y_{12} + H_{22} \Lambda_{23}$$

$$- c_1 H_{22} \Lambda_{25} - c_1 L_{66} \Lambda_{32} + c_1^2 L_{66} \Lambda_{33} - c_1 Y_{66} + c_1^2 O_{66} - c_1 L_{12} \Lambda_{13} + c_1^2 L_{12} \Lambda_{15} - c_1 Y_{12} + c_1^2 O_{12} - c_1 L_{22} \Lambda_{23}$$

$$+ c_1^2 L_{22} \Lambda_{25},$$

$$TB_{35} = H_{66} \Lambda_{32} - c_1 H_{66} \Lambda_{33} + K_{66} - c_1 Y_{66} - c_1 L_{66} \Lambda_{32} + c_1^2 L_{66} \Lambda_{33} - c_1 Y_{66} + c_1^2 O_{66},$$

$$TB_{36} = H_{12} \Lambda_{14} - c_1 H_{12} \Lambda_{16} + H_{22} \Lambda_{24} - c_1 H_{22} \Lambda_{26} + K_{22} - c_1 Y_{22} - c_1 L_{12} \Lambda_{14} + c_1^2 L_{12} \Lambda_{16} - c_1 L_{22} \Lambda_{24}$$

$$+ c_1^2 L_{22} \Lambda_{26} - c_1 Y_{22} + c_1^2 O_{22},$$

$$TB_{37} = -H_{66} \Lambda_{31} - H_{12} \Lambda_{12} + H_{22} \Lambda_{21} + c_1 L_{66} \Lambda_{31} + c_1 L_{12} \Lambda_{12} - c_1 L_{22} \Lambda_{21},$$

$$TB_{38} = H_{12} \Lambda_{11} - H_{22} \Lambda_{12} - c_1 L_{12} \Lambda_{11} + c_1 L_{22} \Lambda_{12}.$$

Appendix B

$$\begin{aligned}
sa_{11} &= -k_1 - k_2(\lambda_m^2 + \delta_n^2) + TB_{13}\lambda_m^4 + TB_{14}\lambda_m^2\delta_n^2 + TB_{15}\delta_n^4 + TB_{110}P_1\lambda_m^4 + TB_{111}P_1\lambda_m^2\delta_n^2 + TB_{112}P_1\delta_n^4, \\
sa_{12} &= -TB_{11}\lambda_m + TB_{16}\lambda_m^3 + TB_{17}\lambda_m\delta_n^2 + TB_{110}P_2\lambda_m^4 + TB_{111}P_2\lambda_m^2\delta_n^2 + TB_{112}P_2\delta_n^4, \\
sa_{13} &= -TB_{12}\delta_n + TB_{18}\delta_n^3 + TB_{19}\lambda_m^2\delta_n + TB_{110}P_3\lambda_m^4 + TB_{111}P_3\lambda_m^2\delta_n^2 + TB_{112}P_3\delta_n^4, \\
sa_{14} &= \frac{32P_2\lambda_m\delta_n}{3ab}, sa_{15} = \frac{32P_3\lambda_m\delta_n}{3ab}, y_1 = -TB_{11}\lambda_m^2 - TB_{12}\delta_n^2, y_2 = \frac{32P_1\lambda_m\delta_n}{3ab}, \\
y_3 &= -\frac{8TB_{110}\lambda_m\delta_n}{3ab\Lambda_{21}} - \frac{8TB_{112}\lambda_m\delta_n}{3ab\Lambda_{11}}, y_4 = -\frac{\lambda_m^4}{16\Lambda_{11}} - \frac{\delta_n^4}{16\Lambda_{21}}, y_5 = \frac{16}{mn\pi^2}, \\
sa_{21} &= -\lambda_m^3(TB_{22} + P_1TB_{27}) - \lambda_m\delta_n^2(TB_{23} + P_1T_{28}), \\
sa_{22} &= TB_{21} - TB_{24}\lambda_m^2 - TB_{25}\delta_n^2 - TB_{27}P_2\lambda_m^3 - TB_{28}P_2\lambda_m\delta_n^2, \\
sa_{23} &= -TB_{26}\lambda_m\delta_n - TB_{27}P_3\lambda_m^3 - TB_{28}P_3\lambda_m\delta_n^2, y_6 = TB_{21}\lambda_m, y_7 = \frac{8TB_{27}\delta_n}{3ab\Lambda_{21}}, sa_{31} = -\delta_n^3(TB_{33} + P_1TB_{38}) \\
&\quad - \lambda_m^2\delta_n(TB_{32} + P_1TB_{37}), sa_{32} = -TB_{34}\lambda_m\delta_n - TB_{38}P_2\delta_n^3 - K_{37}P_2\lambda_m^2\delta_n, sa_{33} = TB_{31} - TB_{35}\lambda_m^2 - TB_{36}\delta_n^2 \\
&\quad - TB_{38}P_3\delta_n^3 - TB_{37}P_3\lambda_m^2\delta_n, y_8 = TB_{31}\delta_n, y_9 = \frac{8TB_{38}\lambda_m}{3ab\Lambda_{11}}.
\end{aligned}$$

Appendix C

$$\begin{aligned}
g_1 &= \frac{(\Lambda_{21}a_1 + \Lambda_{12}a_4)}{ab(\Lambda_{12}^2 - \Lambda_{11}\Lambda_{21})} \frac{4}{\lambda_m\delta_n}, g_4 = -\frac{1}{8} \frac{(\Lambda_{21}\lambda_m^2 + \Lambda_{12}\delta_n^2)}{(\Lambda_{12}^2 - \Lambda_{11}\Lambda_{21})}, g_2 = \frac{(\Lambda_{21}a_2 + \Lambda_{12}a_5)}{ab(\Lambda_{12}^2 - \Lambda_{11}\Lambda_{21})} \frac{4}{\lambda_m\delta_n}, \\
g_3 &= \frac{(\Lambda_{21}a_3 + \Lambda_{12}a_6)}{ab(\Lambda_{12}^2 - \Lambda_{11}\Lambda_{21})} \frac{4}{\lambda_m\delta_n}, g_5 = \frac{(\Lambda_{17}\Lambda_{21} + \Lambda_{27}\Lambda_{12})}{(\Lambda_{12}^2 - \Lambda_{11}\Lambda_{21})}, g_6 = \frac{(\Lambda_{18}\Lambda_{21} + \Lambda_{28}\Lambda_{12})}{(\Lambda_{12}^2 - \Lambda_{11}\Lambda_{21})} \\
f_1 &= \frac{(a_1\Lambda_{12} + \Lambda_{11}a_4)}{ab(\Lambda_{12}^2 - \Lambda_{11}\Lambda_{21})} \frac{4}{\lambda_m\delta_n}, f_4 = -\frac{1}{8} \frac{(\lambda_m^2\Lambda_{12} + \Lambda_{11}\delta_n^2)}{(\Lambda_{12}^2 - \Lambda_{11}\Lambda_{21})}, f_2 = \frac{(a_2\Lambda_{12} + \Lambda_{11}a_5)}{ab(\Lambda_{12}^2 - \Lambda_{11}\Lambda_{21})} \frac{4}{\lambda_m\delta_n}, \\
f_3 &= \frac{(a_3\Lambda_{12} + \Lambda_{11}a_6)}{ab(\Lambda_{12}^2 - \Lambda_{11}\Lambda_{21})} \frac{4}{\lambda_m\delta_n}, f_5 = \frac{(\Lambda_{17}\Lambda_{12} + \Lambda_{11}\Lambda_{27})}{(\Lambda_{12}^2 - \Lambda_{11}\Lambda_{21})}, f_6 = \frac{(\Lambda_{18}\Lambda_{12} + \Lambda_{11}\Lambda_{28})}{(\Lambda_{12}^2 - \Lambda_{11}\Lambda_{21})} \\
a_1 &= (-\Lambda_{11}\delta_n^2P_1 + \Lambda_{12}P_1\lambda_m^2 + c_1\Lambda_{15}\lambda_m^2 + c_1\Lambda_{16}\delta_n^2), a_2 = ((-\Lambda_{13} + c_1\Lambda_{15})\lambda_m + \Lambda_{12}P_2\lambda_m^2 - \Lambda_{11}P_2\delta_n^2) \\
a_3 &= ((-\Lambda_{14} + c_1\Lambda_{16})\delta_n + P_3\Lambda_{12}\lambda_m^2 - \Lambda_{11}P_3\delta_n^2), a_4 = (-P_1\Lambda_{21}\lambda_m^2 + \delta_n^2P_1\Lambda_{12} + c_1\Lambda_{26}\delta_n^2 + c_1\Lambda_{25}\lambda_m^2) \\
a_5 &= ((-\Lambda_{23} + c_1\Lambda_{25})\lambda_m + \Lambda_{12}P_2\delta_n^2 - \Lambda_{21}P_2\lambda_m^2), a_6 = ((-\Lambda_{24} + c_1\Lambda_{26})\delta_n + \Lambda_{12}P_3\delta_n^2 - \Lambda_{21}P_3\lambda_m^2) \\
sa_{14}^1 &= (s_{1a4} - \lambda_m^2g_2 - \delta_n^2f_2), sa_{15}^1 = (sa_{15} - \lambda_m^2g_3 - \delta_n^2f_3), y_1^1 = \begin{bmatrix} y_1 - (\lambda_m^2g_5 + \delta_n^2f_5)\Phi_1 \\ -(\lambda_m^2g_6 + \delta_n^2f_6)\Phi_2 \end{bmatrix} \\
y_2^1 &= (y_2 - \lambda_m^2g_1 - \delta_n^2f_1), y_4^1 = (y_4 - \lambda_m^2g_4 - \delta_n^2f_4)
\end{aligned}$$